UNIVERSITY OF HELSINKI REPORT SERIES IN ASTRONOMY

No. 16

Variability of young solar-type stars: Spot cycles, rotation, and active longitudes

Jyri Lehtinen

Academic dissertation

Department of Physics
Faculty of Science
University of Helsinki
Helsinki, Finland

To be presented, with the permission of the Faculty of Science of the University of Helsinki, for public criticism in Physicum auditorium E204 on April 7th, 2016, at 12 o'clock noon.

Helsinki 2016

Supervisors:	Docent Lauri Jetsu Department of Physics University of Helsinki
	Docent Thomas Hackman Department of Physics University of Helsinki
Pre-examiners:	Prof. Ilya Usoskin Sodankylä Geophysical Observatory & Department of Physics University of Oulu
	Dr. Steven Saar Harvard-Smithsonian Center for Astrophysics
Opponent:	Prof. Hans Kjeldsen Department of Physics and Astronomy Aarhus University
Custos:	Prof. Karri Muinonen Department of Physics University of Helsinki

Cover picture: Acquisition frame of the active star LQ Hya observed for spectroscopic centering at the Nordic Optical Telescope. LQ Hya is the bright star on the lower left of the frame.

ISSN 1799-3024 (print version)
ISBN 978-951-51-1578-2 (print version)
Helsinki 2016
Helsinki University Print (Unigrafia)

ISSN 1799-3032 (pdf version)
ISBN 978-951-51-1579-9 (pdf version)
ISSN-L 1799-3024
http://ethesis.helsinki.fi/
Helsinki 2016
Electronic Publications @ University of Helsinki
(Helsingin yliopiston verkkojulkaisut)

Jyri Lehtinen: **Variability of young solar-type stars: Spot cycles, rotation, and active longitudes**, University of Helsinki, 2016, 57 p. + appendices, University of Helsinki Report Series in Astronomy, No. 16, ISSN 1799-3024 (print version), ISBN 978-951-51-1578-2 (print version), ISSN 1799-3032 (pdf version), ISBN 978-951-51-1579-9 (pdf version), ISSN-L 1799-3024

Keywords: stellar activity, solar-type stars, starspots, time series analysis

Abstract

The outer convective envelopes of late-type stars, including our Sun, are believed to support turbulent dynamos that are able to generate strong and dynamic magnetic fields. When these magnetic fields penetrate the stellar surface, they give rise to a variety of activity phenomena which can be directly observed. These include dark spots on the stellar photospheres as well as bright line emission originating in the chromospheric layers. Observing and analyzing these activity indicators allows us to characterize the behaviour of the dynamos on a wide range of different stars. It also makes it possible to place the activity behaviour of the Sun into a wider context, thus helping to further our understanding of the solar activity and its impact to our local space.

This thesis presents a study of the activity behaviour of a sample of 21 young solar-type stars that can be seen as analogues of the Sun during the first few hundred million years of its existence. The analysis aims to characterize the activity behaviour of the sample stars on different time scales from months to decades as well as to derive estimates for the magnitude of their surface differential rotation. The results of the analysis provide important observational constraints for the dynamo theory.

The study is primarily based on the time series analysis of up to three decades of photometric monitoring of the sample stars. The light curves of these stars display quasiperiodic variations that are induced by changing patterns of dark starspots on the stellar surface and the rotation of the star. As a star rotates, the spots on its surface disappear and reappear periodically, making it possible to determine the rotation period and to quantify the spot distribution. This task is achieved by fitting the observed light curves with periodic models and deriving descriptive parameters from these. The time series analysis results are supplemented by spectroscopic observations that are used to determine the chromospheric activity levels of the stars.

The time series analysis is performed using the Continuous Period Search and Carrier Fit methods along with a selection of additional complementary tools. The development of the Continuous Period Search method forms a part of this thesis. This method is fully characterized and its performance is tested on noisy low amplitude light curve data.

The photometric analysis reveals new results from both activity cycles and the longitudinal distribution of the spot activity on the stars. Furthermore, it confirms previously published results concerning these and the strength of the surface differential rotation using a new sample of stars. The results show that activity cycles of different lengths are common on active solar-type stars. When their lengths are investigated in relation to the rotation rates or chromospheric activity levels of the stars, the detected cycles fall on a clearly defined set of branches, suggesting the excitation of different cyclic modes in the dynamos. The results of the current study reveal a previously undescribed split of cycle lengths into two parallel branches with some stars having

simultaneously detected cycles on both of them.

When the longitudinal distribution of the spot activity is compared to the rotation rate or the activity level of the stars, the results show a clear domain shift between stars that have axisymmetric spot distributions and stars where the spot activity shows stable longitudinal concentration. Such concentration of activity, known as active longitudes, only appears on the faster rotating more active stars. This suggests a transition between axisymmetric and non-axisymmetric dynamo modes in the active stars as a function of their activity level. When active longitudes are seen, they show a tendency to follow prograde propagation in the stellar rotational frame of reference. This may be interpreted either as a signature of radial differential rotation, if the active longitude structures are anchored somewhat below the visible stellar surface, or as an azimuthal dynamo wave, if the active longitudes are fully decoupled from the plasma flow.

Acknowledgements

This thesis could not have become a reality without the support and input of my supervisors Dr. Lauri Jetsu and Dr. Thomas Hackman who introduced me to the fields of stellar activity and time series analysis all the way back during writing my bachelor's thesis. I am grateful for their practical support and the insightful discussions I have had with both of them. A third instrumental person in the success of my thesis research has been Gregory Henry from the Tennessee State University. He has generously provided us with the long time series of stellar photometry and given us good critical feedback when writing our papers.

Several more people who deserve to be thanked include in particular Dr. Heidi Korhonen, Dr. Jaan Pelt, Dr. Maarit Käpylä, and Prof. Axel Brandenburg. The discussions I have had with them have been helpful for developing my understanding in observational astronomy, time series analysis, and stellar activity. Furthermore, I wish to thank my pre-examiners Prof. Ilya Usoskin and Dr. Steven Saar for their positive comments on this thesis.

During my PhD studies I spent one year working at the Nordic Optical Telescope on the island of La Palma in the Canaries. I cannot overemphasize how well the telescope manages to provide a first class environment for learning practical observational astronomy. Working at the telescope was a major influence for me to ultimately include spectroscopy in this thesis in addition to the photometric work that forms the majority of it. I also enjoyed greatly the astronomer community on the island and learned to know many wonderful people there. Returning to the island is always a great pleasure for me.

The University of Helsinki has been quite an environment to study physics and grow into the academia. I have definitely encountered a full spectrum of colourful university life while studying here (Mézières & Christin, 1998). Many thanks especially to all my friends in the student life for the excellent ride. We will have plenty of things to remember from our time for the years to come.

I must ultimately thank my family for sparking in me the interest in astronomy and supporting me in pursuing the field as an actual profession. I have still kept astronomy as a pastime interest as well and, again, I am grateful for getting to meet so many excellent people in the Finnish amateur astronomy community. I feel that doing the occasional visual observations of the Sun and other celestial objects has been helpful for giving me a personal connection to my research. Among the targets that I have observed on the sky are some of the young star clusters which include the active stars of my study as their members.

ἐν δὲ τὰ τείρεα πάντα, τά τ᾽ οὐρανὸς ἐστεφάνωται,
Πληϊάδας θ᾽ Ὑάδας τε τό τε σθένος Ὠρίωνος
Iliad, 18:485–486

List of publications

Paper I: J. Lehtinen, L. Jetsu, T. Hackman, P. Kajatkari, and G. W. Henry, 2011, "The continuous period search method and its application to the young solar analogue HD 116956", Astronomy & Astrophysics, 527, A136

Paper II: J. Lehtinen, L. Jetsu, T. Hackman, P. Kajatkari, and G. W. Henry, 2012, "Spot activity of LQ Hydra from photometry between 1988 and 2011", Astronomy & Astrophysics, 542, A38

Paper III: P. Kajatkari, L.Jetsu, E. Cole, T. Hackman, G. W. Henry, S.-L. Joutsiniemi, **J. Lehtinen**, V. Mäkelä, S. Porceddu, K. Ryynänen, and V. Şolea, 2015, "Periodicity in some light curves of the solar analogue V352 Canis Majoris", Astronomy & Astrophysics, 577, A84

Paper IV: N. Olspert, M. J. Käpylä, J. Pelt, E. M. Cole, T. Hackman, **J. Lehtinen**, and G. W. Henry, 2015, "Multiperiodicity, modulations, and flip-flops in variable star light curves. III. Carrier fit analysis of LQ Hydrae photometry for 1982–2014", Astronomy & Astrophysics, 577, A120

Paper V: J. Lehtinen, L. Jetsu, T. Hackman, P. Kajatkari, and G. W. Henry, 2016, "Activity trends in young solar-type stars", Astronomy & Astrophysics, 588, A38

List of abbreviations

APT	Automated Photometric Telescope
BIC	Bayesian Information Criterion
CF	Carrier Fit
Chk	check star
Cmp	comparison star
CPS	Continuous Period Search
DI	Doppler Imaging
NOT	Nordic Optical Telescope
TSPA	Three Stage Period Analysis
Var	variable target star
ZDI	Zeeman Doppler Imaging

Contents

1 Introduction

Magnetic fields are a ubiquitous phenomenon in the universe, observed from the smallest scales up to the very largest ones. It is thus no wonder that we find them in a wide variety of stars and that they have an important role to play in the stellar behaviour and evolution. In late-type stars with convective outer layers, magnetic fields are generated by a dynamo mechanism, supported by the rotation of the star and the turbulent flows of plasma in the convection zone (Charbonneau, 2010). The resulting magnetic fields are highly dynamic and give rise to a variety of observed activity phenomena. These range from dark photospheric spots and bright chromospheric emission, where the concentrated magnetic flux tubes breach the stellar atmosphere, to the explosive events of flares and coronal mass ejections, caused by magnetic reconnection, and to the variability of the hot corona and the stellar wind (Berdyugina, 2005; Hall, 2008). The stellar wind and the high energy radiation caused by the activity phenomena affect the conditions in the circumstellar space and are important considerations for the interaction of a star and its planetary system (Vidotto et al., 2015). Coupling of the magnetic field with the strong stellar wind is also responsible for transferring angular momentum away from the star, leading to the spin down of young active stars as they age (Soderblom, 1991).

On the Sun, activity phenomena have been known observationally since the antiquity through sporadic observations of the sunspots by naked eye (Usoskin, 2013). It took, however, until the invention of the telescope in the 17th century for the sunspots to be observed more systematically. On stars other than the Sun, dark starspots were first correctly interpreted to exist by Kron (1947) from the changing out of eclipse variation of the binary AR Lac. Emission originating from the chromospheres of other stars had already been observed earlier by Eberhard & Schwarzschild (1913), including on the very active binary σ Gem. More systematic studies of the stellar chromospheric and spot activity were begun starting from the 1960's (see e.g. Wilson, 1978; Henry et al., 1995).

The link between the observed activity phenomena and magnetic fields is not a trivial one to make. The connection of sunspots to the presence of strong magnetic fields on the Sun was not made until the early 20th century by Hale (1908) from the Zeeman splitting seen in several photospheric spectral lines. Currently magnetic fields have been directly measured from a number of stars and even the magnetic field geometries have been mapped on many of them using the procedure of Zeeman Doppler imaging (Morin et al., 2011; Marsden et al., 2014). However, because of the demanding observational requirements needed for the measurement of stellar magnetic fields, it is still most common to study the magnetic activity by more indirect means.

Both time series photometry for studying the spot coverage and spectroscopy for measuring the level of the chromospheric activity are well tested and widely used methods to study the activity of a star. Time series photometry in particular allows for the relatively straight forward determination of the stellar rotation period and the estimation of the differential rotation. It can also be used for searching activity cycles,

akin to the 11 year spot cycle of the Sun, and other possible regularities present in the distribution of the starspots. Measurements of the chromospheric emission level by high resolution spectroscopy will furthermore directly provide useful estimates of the activity level of a star.

Despite the fact that activity related phenomena have been studied on stars other than the Sun already for several decades, most of our knowledge of stellar magnetism is still based on observations of the Sun. The current models to explain the stellar dynamos are thus bound to be skewed towards the solar behaviour. In order to improve the models, it is necessary to gather more data of the occurrence of the activity phenomena from a wider sample of stars. Observing the activity of solar-type stars with different activity levels is in particular useful since it can provide data from a wide range of activity behaviours from stars that can easily be compared with the Sun.

The object of this thesis is to study the spot activity on such a sample of young solar analogues using time series photometry. The stars in the sample are effectively single and have ages ranging from a few million to half a billion years. They belong to the spectral types F, G, and K, meaning that their internal structure consists of a radiative core and a convective outer envelope. Thus, they can be considered as analogues of the young Sun and it is reasonable to assume that their activity reflects that of the Sun during the early years of its development. Studying these stars will then provide valuable information from the evolution of the activity of the Sun through its life as well as from the conditions in the early solar system.

The thesis is structured as follows. In Chapter 2, a general review is given of the various phenomena related to stellar activity and in particular the occurrence of starspots. Basic essentials to consider for dynamo theories are also briefly covered. Chapter 3 provides a more detailed discussion of the photometric and spectroscopic methods used for studying stellar activity which are relevant for the current study, while the time series analysis methods used for the photometric data are covered in Chapter 4. Results obtained with these methods are then discussed in Chapter 5. Finally, Chapters 6 and 7 provide summaries of the papers constituting the thesis and a concluding discussion with future prospects.

2 Stellar magnetic activity

2.1 Forms and origin of stellar activity

There is a large variety of phenomena connected to magnetic activity which have been observed on the Sun and other active stars. On the Sun perhaps the most visually striking ones are the sunspots. These are locations on the photosphere where strong magnetic flux tubes penetrate the solar surface. The magnetic fields with a strength of several kilogauss in the flux tubes suppress locally the convective heat transport leading to cooler and darker areas in the photosphere. The individual sunspots occur in active areas, which form as larger more concentrated magnetic loops rise above the photosphere. In larger and better developed sunspot groups this leads to a bipolar structure where the spots at the opposite ends of the group show opposite magnetic polarities. Associated to the spots, the active regions also include bright network-like faculae. These are areas where the strengthened magnetic field causes moderate heating of the surface plasma but is not strong enough to cause the formation of spots.

Above the solar photosphere lies the chromosphere, which is likewise a location for several activity phenomena. These become immediately visible when observing the Sun at the wavelengths of strong spectral lines which have their cores formed within the chromosphere. Fig. 2.1 shows an example image of the Sun observed at the wavelength of the Hydrogen Hα line. In addition to sunspots, there are bright chromospheric regions, or plages, corresponding to the photospheric faculae. Also evident are prominences rising above the solar limb or visible as dark filaments over the brighter chromosphere. These consist of chromospheric plasma supported in the hot but diluted transition region and inner corona of the Sun by the magnetic loops penetrating through the solar surface. Occasionally the loops become tightly entangled, leading to explosive reconnection events and the release of massive amounts of magnetic energy in flares. These are themselves complex phenomena, observed over the electromagnetic spectrum from radio, across the visible spectrum both in photospheric continuum and chromospheric line emission, to X-ray and gamma emission from the superheated plasma.

It is far from straight forward to observe the activity on other stars than the Sun. Nevertheless, despite their large distances, the same activity phenomena can be identified on them. These include starspots, corresponding to the sunspots, chromospheric activity, and flares. The coronae of active stars can furthermore be observed in radio, far ultraviolet, and X-ray emission. Connecting these phenomena to magnetic fields, as in the case of the Sun, is not only based on theoretical reasoning. Observing the Zeeman effect in spectral lines has allowed the direct detection of magnetic fields in the active stars (Donati et al., 1992). The activity of other stars can naturally not be observed in as great detail as the solar activity, and stars with similar activity levels than the Sun pose problems even for the mere detection of the activity. There is, however, much more variation seen in the stars and in many cases the observed activity levels are far above what is seen on the Sun. The sizes of starspots can, for example, be vast compared to sunspots (see e.g. Korhonen et al., 1999; Hackman et al., 2012).

Figure 2.1: The Sun imaged in Hα light showing both sunspots and chromospheric activity features. (Image credit: Samuli Vuorinen)

Magnetic activity has been confirmed for a wide range of stars (Hall, 1991). These range from young pre-main-sequence stars to old giants and belong to the cooler stars with spectral types from F to M. The two major classes of stars on which spot and chromospheric activity have been observed are the BY Dra and the RS CVn stars, named after their prototypes. BY Dra stars are a label often given to young fast rotating main sequence stars that show signs of activity (Bopp & Fekel, 1977). These stars can be either single or binary. Many of them are thought to resemble the Sun at a young age. The RS CVn stars are close active binaries where the primary component can also be a giant star (Hall, 1976). They have commonly fast rotation periods due to tidal forces synchronizing their rotation with the orbital period. A third important class of active stars are the FK Com stars. These are highly active single giants or subgiants with unexpectedly fast rotation. It has been suggested that their fast rotation may be a result of them being coalesced W UMa contact binaries and that they would represent only short transient phases in the development of these systems (Bopp & Stencel, 1981). The FK Com stars are accordingly rare objects and only a few have been conclusively

identified.

The large scale magnetic fields generating the activity phenomena observed on late-type stars must be sustained by some dynamo mechanism. Without such a mechanism the fields would quickly dissipate due to the turbulent diffusion in the convection zones. In mean-field magnetohydrodynamics (Krause & Rädler, 1980) the generation of the poloidal magnetic field component from the toroidal one is described by the α-effect, which parametrizes the helical turbulence. The generation of the toroidal component from the poloidal one is governed both by the α-effect and the shear flows due to differential rotation (Charbonneau, 2010). Hence, it is necessary to know both the state of the differential rotation and the turbulent convection in a star in order to model its dynamo. The relative strengths of the α and the differential rotation terms in the generation of toroidal field affect the behaviour of the dynamo. There is thus a sequence of possible dynamo types from differential rotation dominated $\alpha\Omega$ dynamos to more turbulence dominated $\alpha^2\Omega$ and α^2 dynamos (Ossendrijver, 2003).

The bulk rotation rate of the star is also an important factor in determining the efficiency of magnetic field generation by the dynamo. Hall (1991) observed that above a certain rotation rate late-type stars quickly develop periodic brightness variations indicative of starspot activity in their photospheres. The impact of rotation is characterized by the Rossby number Ro, which is alternatively defined either as the inverse of the Coriolis number, $\mathrm{Ro} = \mathrm{Co}^{-1} = (2\Omega\tau_c)^{-1}$, or simply as the ratio of the stellar rotation period to the convective turnover time, $\mathrm{Ro}' = P_{\mathrm{rot}}/\tau_c$ (see Ossendrijver, 2003). Here τ_c is the theoretically predicted turnover time for the stellar convection zone, and the relation between the rotation period P_{rot} and angular velocity Ω is $P_{\mathrm{rot}} = 2\pi/\Omega$. Hall (1991) determined the onset of strong spot activity to occur approximately at $\mathrm{Ro}' = 2/3$. Moreover, the observed emission flux at the Ca II H and K spectral lines due to chromospheric activity is inversely correlated to Ro (Noyes et al., 1984). Observations from solar active regions have shown a power law dependence of both X-rays and the chromospherically originating line emission from photospheric magnetic field strengths (Schrijver et al., 1989). Thus, the rotation rate directly influences the strength of the magnetic fields generated by the dynamos.

The requirements of an outer convection zone and fast enough rotation place restrictions on which type of stars are expected to have magnetic activity. As the dynamo needs a turbulent convection zone to operate, and the generated magnetic fields have to reach the photosphere in order to create observable activity, the typical activity behaviour is restricted to cool late-type stars having convective outer envelopes. Strong fossilized magnetic fields have also been observed on hot early-type stars with radiative outer envelopes and dynamo action in thin sub-surface convective layers had also been proposed for certain cases, but these have to be considered distinct phenomena from the dynamos in the late-type stars (Braithwaite, 2014). The requirement of fast rotation means that strong activity is mostly observed on either young stars or in close binaries with synchronized rotation. The fact that active single stars are mostly young follows from the fact that their magnetic fields couple to their stellar winds, resulting in the expulsion of angular momentum over time (Soderblom, 1991; Collier Cameron et al., 1991). Studies of the rotation of old stars show that there is a sharp decline in the rotation velocities when transitioning from hot stars, which have not had a dynamo, to cool stars, which have had it during some part of their evolution (Gray, 1989). These restrictions in the distribution of activity among the stars are not absolute, as evidenced by the single fast rotating FK Com type giants and certain anomalously slow rotating active stars (Strassmeier et al., 1990), but these are exceptions to the rule.

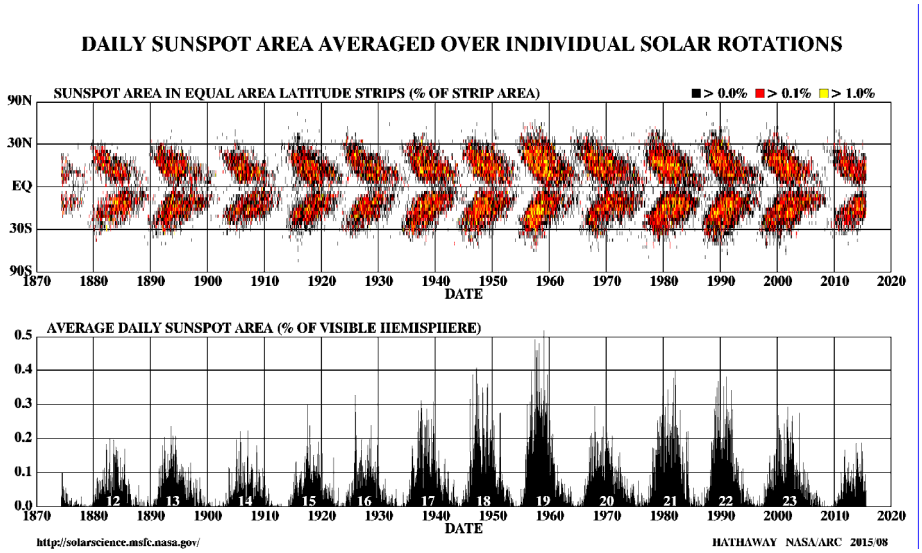

Figure 2.2: The observed sunspot area since 1874 presented against the solar latitude (*top*) and integrated over the whole visible disk (*bottom*). Showing the sunspots against latitude produces the well known butterfly diagram. (Image credit: D. H. Hathaway, NASA/ARC)

2.2 Activity cycles

The solar activity is characterized by the approximately 11 year cycle, discovered by Schwabe (1844), in which the number of sunspots goes up and down. The spot cycle has traditionally been tracked using the rather arbitrary Wolf or Zürich sunspot number

$$R = k\,(10\,g + n), \tag{2.1}$$

where g is the number of sunspot groups, n the number of individual sunspots, and k a correction factor needed for combining observations from different observers. Other more physically motivated proxies have also been used for tracking the activity level of the Sun, including the sunspot group number, the total sunspot area, radio emission at the 10.7 cm wavelength, and the total solar irradiance (Hathaway, 2015). Fig. 2.2 presents the spot cycle between 1874 and 2015 using the observed spot area. Magnetogram observations have shown that the spot cycle is associated with a magnetic polarity reversal between each individual cycle (Hale et al., 1919), revealing the spot cycle to be a manifestation of an approximately 22 year magnetic cycle.

The variation of the activity level and the magnetic reversals are not the only characteristics of the solar cycle. In addition to these, there is an equator-ward migration pattern of the active areas associated with each spot cycle. In the start of a cycle new active regions start to form at mid-latitudes on the Sun. As the cycle progresses, the formation of active regions takes place at lower and lower latitudes, until at the end of the cycle they are formed very near to the equator. The active areas form two bands located symmetrically at the opposite sides of the solar equator. These can be seen in Fig. 2.1 as the two horizontal strips containing all the visible sunspots and plages. The repeating equator-ward migration of the activity bands forms a latitudinal activity

wave which an adequate dynamo model has to be able to reproduce. The activity wave is illustrated on sunspots in the upper panel of Fig. 2.2 and forms the well known butterfly diagram. There is also a weaker pole-ward migration of magnetic field associated with the activity wave (Bumba & Howard, 1965) and connected to the regeneration of the poloidal field of the Sun.

The sunspot record has a considerable length and allows the search for longer time scale patterns as well. The amplitude of the individual cycles is clearly variable with a characteristic timescale of 60 to 140 years, known as the Gleissberg cycle (Gleissberg, 1939). At the start of the sunspot record, between 1645 and 1715, there was also an extended period with few visible spots on the Sun, known as the Maunder minimum (Eddy, 1976). Further grand minima, similar to the Maunder minimum, have been found from long records of abundances of the cosmogenic isotopes ^{14}C and ^{10}Be from tree rings and ice core samples (see Usoskin, 2013).

The study of activity cycles on other stars is affected by the short spans of the available observation records compared to the time scales of the cycle lengths. In some cases longer records can be reconstructed by combining observations from different sources but most often the available records span only a few decades. Still, quasiperiodic activity variations were suggested already by Wilson (1978) for a number of stars from their chromospheric emission. Subsequent research has produced further and more reliable cycle determinations both using spot and chromospheric activity. Still a further possible way that can in principle be used to study the activity cycles is provided by the coupling of magnetic fields to the gravitational quadrupole moment of a star, as proposed by Applegate (1992). The mechanism explains small quasiperiodic orbital period modulations that have been observed on many close eclipsing binaries (Selam & Demircan, 1999).

Observations of the magnetic fields of some active stars have revealed evidence for magnetic polarity reversals similar to the cycle to cycle reversals observed on the Sun. For proposed reversals in the F type main sequence star τ Boo see Fares et al. (2009) and for a reversal of the poloidal field of the young solar analogue HD 29615 compare Waite et al. (2015) and Hackman et al. (2016). Here the overall results are still patchy and more magnetic data is needed to gain a more accurate picture of the stellar magnetic cycles.

2.3 Differential rotation

As a body of fluid with an convective outer layer, the Sun exhibits differential rotation and the same is in general true for other late-type stars as well. The solar surface differential rotation is a well studied phenomenon and its amplitude and functional form has been determined by a number of authors using different rotation proxies (Beck, 2000). The latitude dependence of the rotation law is modelled as

$$\Omega(\theta) = A + B\sin^2\theta + C\sin^4\theta, \tag{2.2}$$

where θ is the latitude on the solar surface and the term proportional to $\sin^4\theta$ is alternatively included or excluded in the modelling. Snodgrass & Ulrich (1990) reported the values of $A = 2.972\ \mu\,\mathrm{rad\,s^{-1}}$, $B = -0.484\ \mu\,\mathrm{rad\,s^{-1}}$, and $C = -0.361\ \mu\,\mathrm{rad\,s^{-1}}$ using Doppler shifts from the photospheric plasma. The observed surface differential rotation depends, however, on the rotation tracers that have been used to measure it (Schröter, 1985). This means that other factors, like the height in the solar atmosphere, are also relevant for the full rotation law.

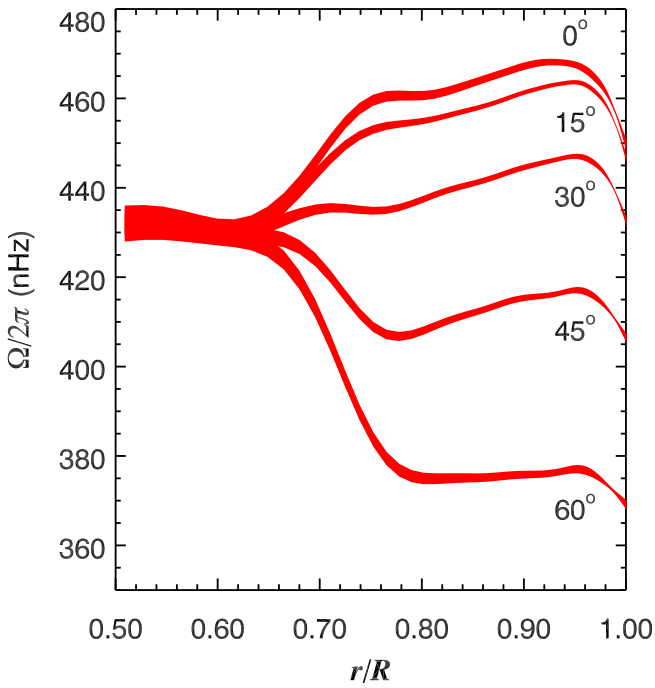

Figure 2.3: The internal rotation of the Sun according to Howe et al. (2000), based on helioseismology. (Image credit: NSF's National Solar Observatory)

Indeed, helioseismology has allowed a detailed look into the internal rotation of the Sun (Howe et al., 2000). The internal rotation profiles resulting from the helioseismic inversion are shown in Fig. 2.3 for five different latitudes. The curves show latitudinal differential rotation throughout the outer convection layer, approximately above the radius $r = 0.7R_\odot$, and rigid body rotation in the radiative core. In addition, there are two layers with notable radial rotational shear. One of them is the tachocline at the bottom of the convection zone, where there is a transition from the rigid body rotation of the core into the distinct latitudinal differential rotation in the convection zone. The other layer with radial differential rotation is just below the surface, where the angular velocity decreases rather uniformly at all latitudes towards the surface. For the bulk of the convection zone the radial differential rotation is quite weak.

Differential rotation is an important parameter for dynamo models and needs to be determined sufficiently. For practical reasons, it is usually reasonable to summarize its amplitude with a single number. This is typically either the relative differential rotation coefficient

$$k = \frac{\Delta\Omega}{\Omega} = \frac{\Omega_{\rm eq} - \Omega_{\rm pol}}{\Omega_{\rm eq}}, \tag{2.3}$$

describing the strength of the differential rotation relative to the equatorial angular velocity $\Omega_{\rm eq}$, or the absolute difference between the equatorial and polar angular velocities, $\Delta\Omega = \Omega_{\rm eq} - \Omega_{\rm pol}$, describing the rotational shear between the equator and the poles. Occasionally also the equatorial to polar lap time $2\pi/\Delta\Omega$ is used. The formulas are defined here for the angular velocity but they can as well be given for the rotation

period.

The surface differential rotation of the Sun is closely modelled by the sinusoid representation (Eq. 2.2) but it is less clear how well this should apply for other stars. Some studies have been made to determine the latitude dependence of the surface rotation on individual stars (e.g. Donati & Collier Cameron, 1997) and the results seem to be favourable for assuming the shape to have general applicability. However, such studies only exist for a few stars and questions can be raised about their robustness. Most often the best that can be done is merely to estimate the magnitude of either k or $\Delta\Omega$. As a result, also the sign of the differential rotation is left undecided in the observations. Theoretical models (Karak et al., 2015) predict solar-like differential rotation, with the poles rotating slower than the equator, for faster rotating stars and anti-solar differential rotation, with the poles rotating faster than the equator, for slower rotating stars. The nature of the transition between the two predicted domains is yet unclear and lacks observational verification. There is, however, robust observational evidence for a temperature dependence of $\Delta\Omega$, so that the thin convective envelopes of the hotter F type stars experience stronger differential rotation than the thicker convective envelopes of the cooler G and K type stars (Reinhold et al., 2013). This is a result also backed by theoretical calculations (Küker & Rüdiger, 2011). Likewise, there is both observational and theoretical evidence that the value of $\Delta\Omega$ is only weakly dependent on the angular velocity of the star.

Apart from differential rotation, there is also a slow systematic pole-ward flow seen on the surface of the Sun (Haber et al., 2000). This is known as the meridional circulation. Helioseismological results have revealed an equator-ward return flow deeper in the convection zone as well as a second circulation cell below the one seen on the surface (Zhao et al., 2013). The meridional circulation is a key ingredient in some dynamo models but so far it has been difficult to observe on any other star except for the Sun (Kővári et al., 2015).

2.4 Active longitudes and flip-flops

On many active stars we observe the activity to concentrate on one or two longitudes and to stay on these locations for extended periods of time (Henry et al., 1995; Jetsu, 1996). The general pattern for these active longitudes is that there is one single longitudinal concentration of activity, or that there are two active longitudes on the opposite sides of the star. The active longitudes can stay stable even for decades in the case of some stars, while on others they appear to experience migration patterns in the longitudinal direction (Korhonen et al., 2002). Such active longitudes have also been suggested to exist on the Sun for flares and sunspots (Bai, 1988; Usoskin et al., 2005), although questions have been raised about the significance of these detections (Pelt et al., 2006). It is worth noting that the strong tidal forces present in close binaries may be an important factor affecting the formation mechanisms of the active longitudes (Holzwarth & Schüssler, 2003). To exclude the potential complications rising from this, only effectively single stars are included in the current study.

Occasionally the active longitudes of a star are observed to experience a flip where the activity changes from one side of the star to the opposite. The change can be complete, so that no activity is left on the original active longitude, or it can be partial, where only the relative strengths of activity switch between the two active longitudes. Such flip-flop events were first seen on the active giant star FK Com (Jetsu et al., 1993). On this star the observations indicated that the spot activity was always concentrated

on one of two active longitudes separated by 180° in longitude. On several occasions the spots had completely disappeared on one active longitude and reformed on the opposite one. Over the years this resulted in a back and forth switching in the activity pattern. It has been suggested that the flip-flops seen on many stars could follow periodic patterns that would resemble the activity cycles (Berdyugina et al., 2002). Further research has shown, however, that the observed flip-flops are unlikely to occur with any discernible periodicity (e.g. Lindborg et al., 2013; Hackman et al., 2013).

Purely observationally defined flip-flops can have different physical interpretations. They may originate from an underlying process where the activity really decreases or vanishes on one active longitude and switches to the other one. On the other hand, observational signals resembling such flip-flops may also arise from a simple beating pattern caused by two spots or active areas at different stellar latitudes moving with different rotation periods. Distinguishing between such cases is not necessarily trivial and some care is necessary when interpreting the nature of flip-flops seen in the data.

As of yet, there is no commonly agreed definition on what phase coherent activity features count as active longitudes. An active longitude needs to have longitudinal coherence but it is not clear for how long it needs to preserve this. As a working definition it can be taken that an active longitude needs to stay intact for at least a couple of years to count as one. Shorter lived phase coherent features may simply be particularly long lived active areas. For flip-flops, a definition was given by Hackman et al. (2013). This definition states that in order to count as a flip-flop, the main location of activity needs to shift 180° from an old active longitude in the longitudinal direction and then stay for a while at its new location. In other words, the activity needs to be concentrated on one or two active longitudes both before and after a flip-flop event. Otherwise the phase shift can simply be the result of active areas forming randomly on all longitudes. No definition is given for the manner in which the switch in longitude has to happen and it can either be an abrupt change or a more gradual process taking weeks or months to happen.

An explanation for the active longitudes is that they are manifestations of non-axisymmetric dynamo modes. These contrast with the axisymmetric modes responsible for the solar-like activity pattern where the activity is in the long run distributed uniformly over all longitudes. The idea is that a non-axisymmetric dynamo mode will generate strong magnetic concentrations on two opposite longitudes on a star and active areas will preferentially be formed around these. Such non-axisymmetric large scale fields are predicted by dynamo theory to occur on fast rotating stars (Tuominen et al., 1999). The non-axisymmetric field configuration does not have to follow exactly the rotation of the stellar plasma and can instead have a differential phase velocity with respect to it. A manifestation of this is that the active longitudes appear to follow a different rotation period than the star itself. Such azimuthal dynamo waves are also predicted by numerical dynamo models (Cole et al., 2014) and can be considered as the longitudinal counterpart to the latitudinal dynamo waves seen on the Sun. The flip-flops, where activity physically switches between the active longitudes, could be connected to magnetic polarity reversals in the non-axisymmetric fields (Tuominen et al., 2002), although the lack of periodicity in their occurrence may pose problems for a direct analogy with the solar magnetic cycle.

3 Observing the stellar activity

Stellar magnetic activity manifests itself in a wide range of different phenomena which can be observed over much of the electromagnetic spectrum. The most commonly used observational methods concentrate on the optical wavelengths and the activity phenomena located in the photospheres and chromospheres of the stars. These are time series photometry, spectroscopy of chromospheric line emission, and Doppler imaging. Here basic principles of these methods are given with special attention to the time series photometry and the chromospheric spectroscopy used in this thesis project.

3.1 Time series photometry

The presence of cool starspots on a star can be inferred from photometric observations. When a spot appears on a star, it causes the apparent brightness of the star to drop and the colour to redden. An individual photometric observation is not enough to decide if the star has spots or not, but since starspots are a time dependent phenomenon, they will become apparent when one gathers longer time series of photometry.

First of all, as a star rotates, the spots on its photosphere will periodically disappear and reappear. This modulates the observed brightness. The spots do not even have to disappear behind the limb of the star to cause visible brightness modulation. Both limb darkening and the changing geometric projection of the spots have a measurable impact on the observed brightness. As a result, higher latitude spots on stars observed at intermediate rotational inclinations will in general also contribute to the brightness modulation despite staying constantly on the visible stellar disk.

Because of this periodicity in the photometric spot signal, the photometry can be used to determine the stellar rotation period. It can furthermore be used to estimate the magnitude of the surface differential rotation. As observed on the Sun, we may assume that spots located at different stellar latitudes follow the differentially rotating surface plasma and display different rotation periods. The range of rotation periods can be retrieved from the photometry, and thus act as a proxy of the differential rotation.

The photometry also contains information about the distribution of the spots on the star. The latitude of a spot will cause it to have different impacts on the observed light curve but, because the shape of the spots or spot groups remains unknown, the latitude remains an ill determined parameter. On the other hand, the longitudes of the spots are easily determined from the rotational phases of the observed light curve minima. The resolving power is limited by the fact that each spot remains on the visible disk for a large fraction of the stellar rotation. This leads to broad light curve minima that blend into each other. In practice, no more than two separate minima can be distinguished simultaneously. However, by modelling the evolution of the light curve, much finer phase resolution can be achieved, making time series photometry useful for the search and characterization of active longitudes.

Lastly, the photometric record is commonly used to track variations of the general level of spottedness as well as the degree of axisymmetry in the spot distribution. These

are tracked by the observed mean brightness and the amplitude and minimum times of the light curve. Especially the mean brightness is a parameter that is sensitive to the long term activity changes of a star and it is commonly used for determining activity cycles.

Studying the spot activity requires long and uniform records of time series photometry. This is especially true if one aims to search and characterise activity cycles, but also studying the long term behaviour of active longitudes requires extended data sets. Such long time series are best achieved by using dedicated robotic telescopes which observe the same stars night after night and can be used for the same monitoring programme for several decades. Many such Automatic Photometric Telescopes (APTs), with apertures ranging from 20 cm to over a meter, have been erected over the past decades and active stars form a significant part of their observing programmes (Berdyugina, 2005).

In the last decade, also space based photometry has become an option for studying spotted stars through the MOST, CoRoT, and Kepler missions. Space based photometry offers a much improved precision compared to what can be achieved with the ground based telescopes. As a result, it is better suited for estimating rotational phenomena, such as the magnitude of the differential rotation. On the other hand, space based instrumentation suffers more calibration difficulties than ground based instrumentation, which makes it difficult or impossible to retrieve the accurate mean brightness of a star and use its variations for searching activity cycles. The space missions have also had shorter time spans than many ground based monitoring programmes, meaning that any longer time scale phenomena, such as decadal activity cycles, are necessarily left outside of their current scope.

For our studies, we have used photometry from the 0.40 m aperture T3 APT operated by the Tennessee State University Automated Astronomy Group[1] at the Fairborn observatory in southern Arizona. The telescope performs nightly photometry of its programme stars through standard Johnson B and V band filters with a photometer using a photomultiplier tube. The stars are found and centred in the diaphragm of the photometer by taking an image of the field with a CCD camera that picks light from the optical axis of the telescope with a rotating mirror. After centring the stars in the diaphragm, the mirror is moved out of the way and the stellar light is collected by the photometer (Henry, 1995).

Each star is observed in a sequence Chk – Sky – Cmp – Var – Cmp – Var – Cmp – Var – Cmp – Sky – Chk, where Var is the variable target star, Chk a constant check star, Cmp a constant comparison star, and Sky a background sky position. This sequence produces two sets of differential photometry, the variable star time series Var − Cmp and a check star time series Chk − Cmp. The sky observations are used to subtract the background sky level from the stellar observations. Monitoring the check star at the same time with the target star allows us to ensure that the chosen comparison star has a constant brightness. As long as the check star photometry stays constant, all the variability seen in the target star photometry can be attributed to the target star.

The final values of differential photometry are obtained as the means of the individual observations within each observing sequence, while the scatter of the observations provides a check for their reliability. The internal precision, i.e. the repeatability of observations within each sequence, of the T3 photometry is typically between 0.0025 and 0.0035 mag when conditions are good. If the scatter of the individual target star observations is greater than 0.01 mag, or about 3σ of the typical internal precision, the

[1] `http://schwab.tsuniv.edu/index.html`

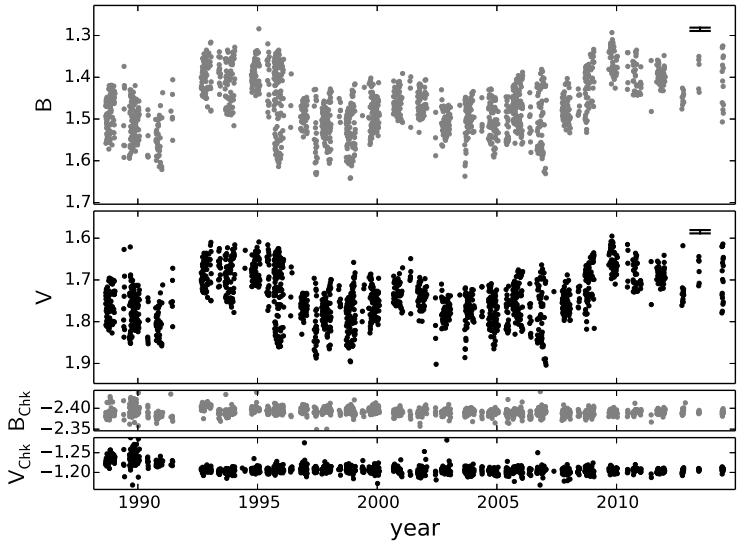

Figure 3.1: Raw differential photometry of the young active solar-type star PW And from the T3 APT in the Johnson B and V bands. The top two panels show the Var − Cmp photometry and the bottom two panels the Chk − Cmp photometry in the same scale. The ±0.004 mag photometric precision is shown with the connected horizontal lines at the top right corners of the Var − Cmp panels.

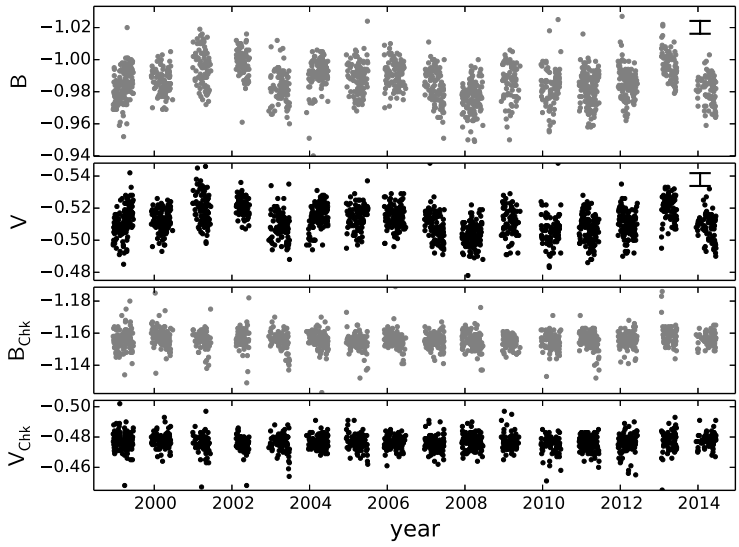

Figure 3.2: Same as Fig. 3.1 but for the low amplitude star HP Boo.

full observing sequence is discarded. The external precision of the photometry can be estimated by observing a constant pair of stars. Before refurbishing the telescope and installing a new precision photometer in early 1992, this was between 0.008 and 0.016 mag, but it improved to a value between 0.003 and 0.004 mag after the new equipment became operational.

An example of data from the T3 telescope is shown in Fig. 3.1. The upper two panels show the B and V band differential photometry from the highly active solar type star PW And. The lower panels show the simultaneously observed check photometry from the constant check star HD 1439 in the same magnitude scale. The high level of spot activity is evident in the PW And photometry as the large spread seen in the seasonal photometry values as compared to the low level of random scatter in the check star photometry. The extended spread is due to the rotational modulation caused by the spots. Also evident is the year to year variation in the level of the mean brightness caused by the varying level of spottedness on the star.

Most active stars followed photometrically are much less active than PW And and reveal a weaker signature of their spots in the photometry. Fig. 3.2 shows the photometry of one such solar type star HP Boo, which has a moderate level of spot activity. Here we still see some year to year variation in the mean brightness of the star, indicating activity variations, but the amplitude is low. Likewise, the seasonal spread of the target star photometry is only slightly larger than the scatter in the check star photometry, meaning that the rotational brightness modulation is only slightly above the noise level.

There are regular gaps in the photometry of each star caused by their seasonal visibility. In addition to this, the observatory is closed and no data are gathered during the summer rainy season from early June to mid-September (Henry, 1999). This divides the photometric record into observing seasons. Additionally, upgrades or technical problems have resulted in some extended breaks or incomplete observing seasons. This was most notable during the upgrades between 1991 and 1992, as seen in the PW And photometry. It is also worth noticing that the check star photometry has not stayed absolutely constant before and after the installation of the new photometer, but there are slight offsets in both of the channels (Fig. 3.1). This calibration problem between the old and new photometer is fortunately minimized when the comparison star is chosen to have a colour as close as possible to the target star. In the case of PW And, the colour difference between it and the comparison star HD 1406 is only $\Delta(B-V)_{\mathrm{Var-Cmp}} = -0.24$ while the colour difference between the check star HD 1439 and the comparison star is as high as $\Delta(B-V)_{\mathrm{Chk-Cmp}} = -1.20$. The remaining miscalibration in the target star photometry is minimal and dwarfed by the spot induced variability in the photometry. Hence, it does not affect the overall quality of the photometric analysis.

3.2 Chromospheric line emission

Higher in the stellar atmospheres we enter the chromosphere where magnetic activity is associated with emission reversals at the cores of strong absorption lines. The excess emission observed in these lines may come from the plage areas and prominences, as well as from occasional flares associated with the photospheric active regions (Hall, 2008).

For a number of spectral lines the cores are formed in the upper atmospheres of F, G, K, and M type stars. These lines have been used in studying the chromospheric

activity of the Sun and other late type active stars. The most commonly used ones are the H and K lines of singly ionised Calcium at 396.8 nm and 393.3 nm and the Hydrogen Hα line at 653.6 nm. In particular the Ca II H&K lines have received a large amount of attention in stellar activity studies ever since the original programme initiated by Olin Wilson at 1966 with the Mount Wilson 100 inch telescope (Wilson, 1978). The programme followed the variations in the Ca II H&K line emission of 91 F, G, K, and M type main sequence stars. It was later moved to the Mount Wilson 60 inch telescope (Vaughan et al., 1978) where it continued until 2003. Currently similar programmes are run with the Solar-Stellar Spectrograph at the High Altitude Observatory in Colorado (Hall & Lockwood, 1995) and the TIGRE telescope at the La Luz observatory in Mexico (Schmitt et al., 2014).

In addition to time series programmes, there have been many surveys studying the levels of chromospheric activity in large samples of stars (e.g. Henry et al., 1996; Gray et al., 2003, 2006; Wright et al., 2004). As an activity indicator, chromospheric emission has the advantage that longer monitoring is not a necessity for finding out the general activity level of a star. It is possible to measure the chromospheric excess emission from a single spectrum of an active star. Strictly speaking, variations in the activity level cause variable chromospheric emission and rotational modulation affects the observed emission levels in the same way as it affects the photometry. However, since the temporal variation seen on individual stars is lower than the range of emission values observed for different stars, even single isolated observations provide useful information on the general activity level of a star (Baliunas et al., 1995).

The spectroscopy used for measuring the chromospheric emission levels of the stars in our study was observed with the FIES spectrograph[2] at the 2.56 m Nordic Optical Telescope (NOT) located on the island of La Palma (Telting et al., 2014). The instrument is a fibre fed échelle spectrograph mounted in a separate thermally and mechanically insulated building apart from the telescope dome. Light is guided from the telescope focus into the spectrograph through a long optical fibre.

The instrument images the spectrum on a CCD chip in multiple overlapping spectral orders. The useable spectral range spans from about 364 nm to between 717 nm and 736 nm depending on the used resolution. Three different spectral resolutions are available at $R = 25000$, $R = 46000$, and $R = 67000$. These are achieved by using optical fibres of different widths or by using an additional narrow slit at the end of the high resolution fibre. For our observations we have used the high resolution setting at $R = 67000$. Our raw spectra were reduced with the FIEStool pipeline, specifically developed for reducing data from FIES. It acts as a front end for external IRAF packages doing the reduction, and handles the raw image calibration, spectral extraction, wavelength calibration, and merging of the spectral orders. After this, we performed continuum normalization for the Ca II H&K line region by fitting a low order polynomial into identified points of continuum on the both sides of the strong lines.

Two normalized example spectra of this region are shown in Fig. 3.3. These exemplify the very active star V383 Lac and the much less active star V774 Tau. In V383 Lac the emission in the Ca II H&K line cores is strong enough to reach above the continuum level outside the broad line wings. An additional sign of high activity is the presence of emission in the Hydrogen Hϵ line at 397.0 nm immediately on the red side of the Ca II H line. This line is possible to see in emission in the most active stars since its location near the centre of the Ca II H line pushes the effective continuum down allowing the chromospheric component to dominate it. V774 Tau is a much more quiet

[2] http://www.not.iac.es/instruments/fies/

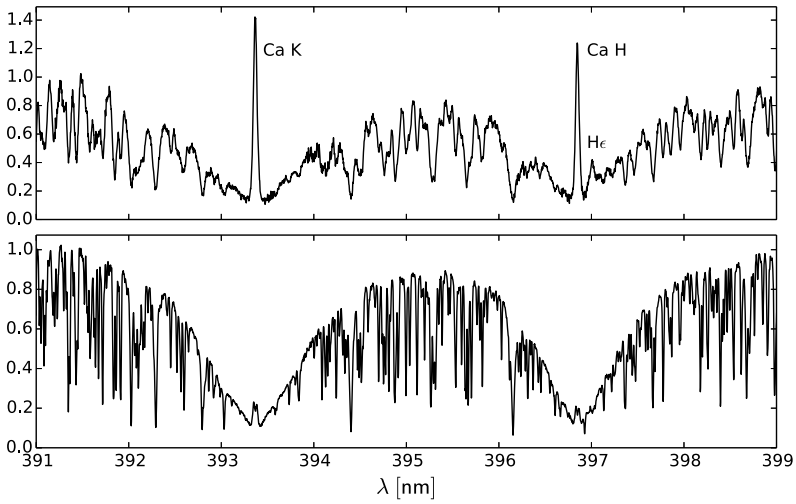

Figure 3.3: FIES spectra from around the Ca II H&K lines of the stars V383 Lac (*top*) and V774 Tau (*bottom*). The spectrum of V383 Lac also shows emission in the Hϵ just beside the Ca II H line core.

star and its Ca II H&K lines show only slight emission with no traces the the Hϵ line. In the case of both of the stars it is apparent how the wavelength regions around and between the Ca II H&K lines are full of weaker absorption lines. This is the case for all late type stars and shows how the continuum normalization of these spectral regions requires some care.

We quantified the chromospheric emission levels of our stars by measuring the Mount Wilson S-index (Vaughan et al., 1978)

$$S = \alpha \frac{H + K}{R + V} \tag{3.1}$$

and transforming it into the fractional emission flux $\log R'_{HK}$ at the Ca II H&K line cores. The standard procedure involves measuring the emission flux in two triangular windows H and K with FWHM 0.109 nm centred at the two line cores. These are compared to the flux measured in two flat continuum windows V and R with full widths of 2.0 nm and centred at 390.1 nm and 400.1 nm on the blue and red sides of the Calcium lines. All the four spectral windows are shown in Fig. 3.4 on top of the spectrum taken from DX Leo. The normalising constant α is needed to adjust the measured values to the same system with the original Mount Wilson HKP-1 and HKP-2 spectrometers. Our observations consisted of single spectra of the active stars, which we decided to calibrate against previously published S values of the same stars by Gray et al. (2003, 2006) and White et al. (2007). The rationale behind using older observations of the same generally variable targets to calibrate newer observations was that over a longer time the mean activity levels of the active stars stay close to the same characteristic levels. Calibration errors due to variable emission levels are furthermore averaged out by using a larger sample of stars for the task. For the normalised FIES spectra we found $\alpha = 19.76$.

The S-indices are transformed into fractional fluxes $R_{\rm HK} = F_{\rm HK}/\sigma T_{\rm eff}^4$ in the line

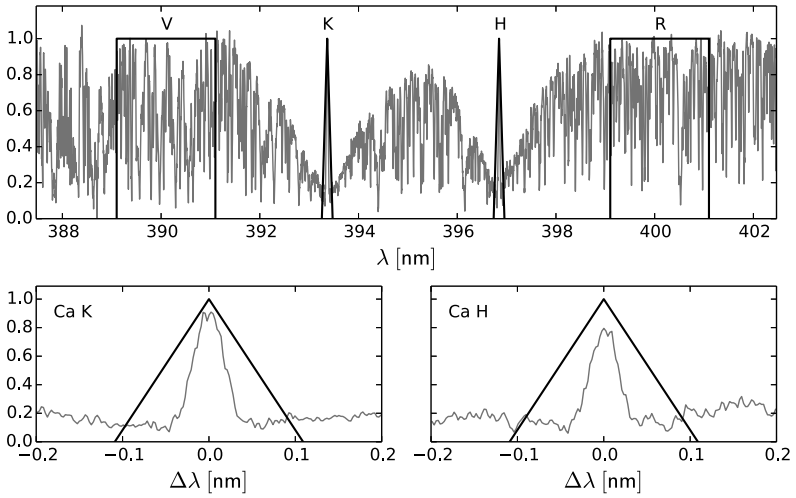

Figure 3.4: The spectral integration windows H, K, V, and R displayed on the spectrum of DX Leo.

cores with respect to the black body luminosity of the stars using the conversion formula (Middelkoop, 1982)

$$R_{\mathrm{HK}} = 1.34 \cdot 10^{-4} C_{\mathrm{cf}} S \tag{3.2}$$

where the colour dependent conversion factor

$$\log C_{\mathrm{cf}} = 0.25\,(B-V)^3 - 1.33\,(B-V)^2 + 0.43\,(B-V) + 0.24 \tag{3.3}$$

is applicable to main sequence stars with $0.3 \leq B-V \leq 1.6$ (Rutten, 1984). This value still contains a photospheric contribution which is described as

$$\log R_{\mathrm{phot}} = -4.898 + 1.918\,(B-V)^2 - 2.893\,(B-V)^3 \tag{3.4}$$

for stars with $B-V \geq 0.44$ (Noyes et al., 1984). This is subtracted from the R_{HK} value to get the final corrected value

$$R'_{\mathrm{HK}} = R_{\mathrm{HK}} - R_{\mathrm{phot}}. \tag{3.5}$$

3.3 Doppler imaging

A second powerful and widely used method for studying stellar activity with high resolution spectroscopy is Doppler imaging (DI; e.g. Vogt et al., 1987; Piskunov et al., 1990). The method is based on the idea that different areas on an inhomogeneous photosphere, such as dark starspots, have different line formation characteristics and continuum contributions to the observed stellar spectrum. The inhomogeneities become visible in the spectral lines where each area on the photosphere produces its own perturbation into the observed line profiles. These perturbations are disentangled from each other by Doppler shifts caused by the stellar rotation. Those formed at the limb of the star rotating towards the observer are shifted to the blue wings of the rotationally broadened spectral lines and those formed at the limb rotating away from the observer

to the red wings of the lines. The stellar rotation further causes these perturbations to migrate across the lines following their changing Doppler shifts, and do this differently depending on their latitude. Hence, observing the changes in the line profiles with an adequate coverage of rotation phases will give information for reconstructing a surface map of the photospheric inhomogeneities.

The surface map X is obtained by minimizing the discrepancy function

$$D(X) = \sum_{\phi,\lambda} \omega_{\phi,\lambda} \frac{\left(r_\phi^{\rm obs}(\lambda) - r_\phi(\lambda)\right)^2}{N_\phi N_\lambda}, \tag{3.6}$$

where ϕ are the N_ϕ rotation phases of the observed spectra, covering each N_λ wavelength points λ with assigned weights $\omega_{\phi,\lambda}$. The discrepancy function measures the difference between the observed normalized spectral profiles $r_\phi^{\rm obs}(\lambda)$ and the normalized model spectra $r_\phi(\lambda)$ computed from the surface map X. The problem of solving X from $D(X)$ is an ill-posed inversion problem, and in the case of noisy data and imperfect phase coverage, a unique solution cannot be found without imposing some additional regularizing constraints for the problem. Common choices have been to either maximize the entropy or the smoothness of the solution X. The additional constraints are implemented by minimizing

$$\Phi(X) = D(X) + \Lambda R(X) \tag{3.7}$$

instead of $D(X)$, where $R(X)$ is the regularization function defining the constraint and Λ is a Lagrangian multiplier.

DI has been used in studying the starspots of late type active stars by mapping their surface temperature or brightness. It has similarly been used for the magnetic Ap stars to produce maps of chemical inhomogeneities. If there is spectropolarimetry available, either including circular polarization or the full Stokes parameters, it is also possible to reconstruct a map of the photospheric magnetic field (e.g. Semel, 1989; Brown et al., 1991). This method is called Zeeman Doppler imaging (ZDI) since it uses the Zeeman effect in the spectral lines as a proxy for the magnetic field.

DI and the photometric analysis are best considered as complementary methods to each other in the study of active stars. When good spectroscopic data is available for DI, it allows the inversion of surface maps containing much more information of the spot distribution than can be inferred from photometry. However, the observations required for producing high quality surface maps are substantially more expensive than time series photometry. The spectroscopy required for DI has to have a high spectral resolution and signal to noise ratio to resolve the low amplitude perturbations in the line profiles. As a result, larger telescopes are needed for the DI observations and it is impossible to get as good coverage for them on as many stars as it is with time series photometry with dedicated telescopes. Moreover, noisy data or poor phase coverage of the observations will introduce artefacts into the surface maps, and the stars are required to have a high enough projected rotational velocity $v \sin i$ for DI to produce reliable results. All this makes the interpretation of the surface maps more complicated than the photometric analysis.

Good surface maps produced by DI provide detailed snapshots of the spot structure while photometry gives a better overall picture of the long-term behaviour of the activity. Most noticeably, photometry is able to bridge the gaps between temporally separated surface maps. ZDI can provide valuable additional information of the configuration of the actual surface magnetic fields, but because of its observational requirements, it has taken more time to become commonly used than regular DI has.

4 Period analysis of time series data

To extract the information available in the photometric records of active stars, we need to use time series analysis and in particular period search methods. For evenly spaced data, basic Fourier analysis provides a natural choice for such a method. Unfortunately, astronomical time series have as a rule unequal spacing, for instance due to nightly and seasonal gaps, and require methods that can take this fact into account. As a result, the Lomb-Scargle periodogram (Lomb, 1976; Scargle, 1982), which is a formulation of the Fourier power spectrum for unequally spaced data, has been immensely popular in astronomical studies.

Period search methods based on Fourier analysis have the disadvantage that they assume a sinusoidal shape for the periodic signal. This is a fair assumption in many cases but in others it can be far from the truth. On spotted stars the presence of multiple spot areas can produce light curves distinctly different from a simple sinusoid. Moreover, a configuration of equally strong spots on the opposite sides of the star will produce a light curve resembling a sinusoid but with a period of only half of the actual rotation period. More specialised and refined approaches have been developed for this kind of situations.

This chapter contains reviews of the methods used in this thesis for analyzing the time series photometry. A number of other methods have also been used for the task by different authors, but since these have not been employed in this thesis, no detailed description is given of them. Such methods include spot modelling using spots of predefined shapes (Budding, 1977; Strassmeier & Bopp, 1992; Fröhlich et al., 2012) and surface map inversion from the light curves (e.g. Messina et al., 1999).

4.1 Three Stage Period Analysis

The Three Stage Period Analysis (TSPA) formulated by Jetsu & Pelt (1999) is one of the more sophisticated and flexible period search methods. Its approach is to use a truncated Fourier series

$$\hat{y}(t_i) = \hat{y}(t_i, \bar{\beta}) = M + \sum_{k=1}^{K} [B_k \cos(k2\pi f t_i) + C_k \sin(k2\pi f t_i)], \tag{4.1}$$

to describe the data y_i at time points t_i. Increasing the model complexity from a simple sinusoid of the standard Fourier analysis allows data with more complex shapes to be analysed reliably. In particular, the more complex model prevents incorrect behaviour when analysing data with more than one minima within its period, as is common in active star photometry.

For period search purposes, the most central of the free harmonic model parameters $\bar{\beta} = [M, B_1, \ldots, B_K, C_1, \ldots, C_K, f]$ is the frequency f or the period $P = f^{-1}$. That said, the model fitting aspect of the method provides further information from the data, enabling a fuller light curve analysis. The mean level of the light curve is directly

modelled by M and the full amplitude A and the epochs $t_{\min}$ of the light curve minima follow from the amplitudes B_k and C_k of the Fourier components. The model order K has to be set before applying the method. In practise, for the smooth active star light curves, $K = 2$ has proven out to be a good choice.

As its name suggests, the TSPA is a multi stage method. Its first stage, the Pilot Search, consists of finding initial guesses for the correct period value by finding the most prominent minima of the phase dispersion spectrum

$$\Theta_{\rm pilot}(f) = \frac{\sum_{i=1,j=i+1}^{n-1,n} Z(\phi_{f,i,j}) W(t_{i,j}) w_{i,j} y_{i,j}}{\sum_{i=1,j=i+1}^{n-1,n} Z(\phi_{f,i,j}) W(t_{i,j}) w_{i,j}} \tag{4.2}$$

over a wide grid of frequency values. These minima correspond to the frequencies which minimize the dispersion between neighbouring data points in the folded data. Here $t_{i,j} = |t_i - t_j|$, $y_{i,j} = (y_i - y_j)^2$, $w_{i,j} = (w_i w_j)(w_i + w_j)^{-1}$, and $\phi_{f,i,j} = {\rm FRAC}(f t_{i,j})$ for the time points t_i, values y_i, and weights w_i of the n individual data points. The function ${\rm FRAC}(x) = x - \lfloor x \rfloor$ denotes the fractional part of its argument x. A natural choice for the weights are the inverse squares of the observational errors, $w_i = \sigma_i^{-2}$.

The Pilot Search offers a quick tool for the initial period search. To boost its efficiency, it uses the additional window functions

$$W(t_{i,j}) = \begin{cases} 1\ , & D_{\min} \le t_{i,j} \le D_{\max} \\ 0\ , & \text{otherwise} \end{cases} \tag{4.3}$$

and

$$Z(\phi_{f,i,j}) = \begin{cases} 1\ , & \phi_{f,i,j} < \tau \\ 1\ , & \phi_{f,i,j} > 1 - \tau \\ 0\ , & \text{otherwise.} \end{cases} \tag{4.4}$$

These filter away the pairs of points which are so close to each other in time that their values will correlate in any case or too far from each other in time or phase that they will not provide useful contribution to the calculation of $\Theta_{\rm pilot}(f)$. The window functions depend of the control parameters $D_{\min}$, $D_{\max}$, and τ which can be tuned to provide optimal performance. In the TSPA these are typically set to $D_{\min} \approx 0.9 f_{\max}^{-1}$, $2 f_{\min}^{-1} \le D_{\max} \le 10 f_{\min}^{-1}$, and $\tau = (4K)^{-1}$, where $f_{\min}$ and $f_{\max}$ are the minimum and maximum frequencies in the test frequency grid.

After the initial stage, the full harmonic model (Eq. 4.1) is taken in the second stage, the Grid Search, and fitted to the data by minimizing the least squares periodogram

$$\Theta_{\rm grid}(f) = 2\, \frac{\sum_{i=1}^{n} w_i [y_i - \hat{y}(t_i, \bar{\beta}_f)]^2}{\sum_{i=1}^{n} w_i} \tag{4.5}$$

In the Grid Search the curve fitting problem is linearized by using constant test frequencies f and performing linear least-squares fitting for the rest of the parameters $\bar{\beta}_f = [M, B_1, \ldots, B_K, C_1, \ldots, C_K]$. The test frequencies are selected from narrower and denser search grids around the best candidate frequencies detected in the Pilot Search. The frequencies producing the best fits are then further taken to the third stage, the Refined Search, where the full nonlinear curve fitting problem is solved by nonlinear least-squares fitting for the full set of model parameters $\bar{\beta}$.

The errors of each of the model parameters are calculated using the bootstrap procedure. This involves calculating the residuals

$$\epsilon_i = y_i - \hat{y}(t_i) \tag{4.6}$$

of the original data against the model fit, forming new "fictive" data $y_i^* = \hat{y}(t_i) + \epsilon_i^*$ from a random sample ϵ_i^* of the residuals, and performing the model fitting for it. A sufficient sample of the bootstrap iterations will produce a distribution of estimates for each of the model parameters so that the standard deviations of these distributions correspond to the error estimates of the parameters. The residual and bootstrap distributions further offer a way to test if the obtained results are reliable. If any one of these is found out to be non-Gaussian with the Kolmogorov-Smirnov test at a significance level of $Q \geq 0.01$, the results of the full period analysis are deemed unreliable.

4.2 Continuous Period Search method

The Continuous Period Search method (CPS; Lehtinen et al., 2011, hereafter Paper I) is a refinement of the TSPA method. Its procedure follows the TSPA and incorporates a number of new features. It also omits the Pilot Search stage of the TSPA and jumps directly to the Grid Search centred around one initial period guess. The lack of a wide initial period search is justified since, when doing period analysis for previously studied astronomical targets, the period of the data is already roughly known. If no previous period determinations exist, a preliminary period search can always be done. We have used the TSPA in such cases for finding the initial period guess.

The first addition in the CPS compared to the TSPA is the way in which longer records of data are divided into shorter manageable datasets. In the TSPA there is no procedure for dividing the data into short datasets and this has to be done separately before the period analysis, when one wishes to study the time evolution of the light curve. The CPS, on the other hand, performs an automatic dataset division before proceeding to the period analysis. The length of these datasets is controlled by the parameter $\Delta T_{\max}$ so that a dataset beginning at a data point t_1 will include all following data points within the time interval $[t_1, t_1 + \Delta T_{\max}]$.

Moreover, the CPS allows a more movie like view of the period analysis results due to a sliding window approach. It allows the datasets to overlap and starts a new one either at each new data point or at each night with new observations. The new dataset is accepted if both it and the previous dataset include data points not found in the other dataset, or equivalently

$$\mathrm{SET}_k \not\subset \mathrm{SET}_{k+1} \text{ and } \mathrm{SET}_{k+1} \not\subset \mathrm{SET}_k. \tag{4.7}$$

A minimum amount of data points, $n_{\min}$, is also required for the datasets to be accepted in order to ensure stable model optimization. As a result of including overlapping datasets in the analysis, there is inherent correlation between the light curve fit results from datasets close to each other. To define a selection of statistically independent datasets suitable for further statistical analyses, a selection of non-overlapping datasets is labelled as "independent" starting from the beginning of the data. It has to be noted that the selection of these independent datasets is arbitrary as long as they do not contain any mutual data points, and many possible selection combinations exist.

The second addition incorporated in the CPS is an objective way to determine the optimal model order K used for the harmonic light curve model (Eq. 4.1). In the TSPA the model order is simply fixed and the same order is used for all datasets being analysed. In practice the changing spot patterns on an active star cause the complexity of the light curve to change in time so that some times a simple sinusoidal model is adequate while other times higher order models are needed. Moreover, especially for the less active low amplitude stars, such as V352 CMa, the light curve amplitude

occasionally dips below the noise level of the data, leading to a constant brightness model, $K = 0$, to be the most suitable way for describing it (Kajatkari et al., 2015, hereafter Paper III). We would optimally want to use a sufficiently complex light curve model for each dataset to fully describe them, but at the same time we want to avoid overfitting, especially in the cases where the data is dominated by noise. This naturally leads to changing the model order K dynamically between the datasets.

To determine the optimal order K of the light curve model, the CPS uses the Bayesian information criterion (BIC, Stoica & Selén, 2004),

$$R_{\mathrm{BIC}} = 2n \ln \sigma_\epsilon^2 + (5K + 1) \ln n, \tag{4.8}$$

where $\sigma_\epsilon^2 = \sum_{i=1}^{n} w_i \epsilon_i^2 \big[\sum_{i=1}^{n} w_i \big]^{-1}$, and the weights are $w_i = \sigma_i^{-2}$, as in the preceding model fitting stages. The criterion consists of two terms where the first is proportional to the logarithmic likelihood of the model fit. In the case of the CPS, it is defined for residuals with a Gaussian distribution. The second term is a penalty term which increases for higher model orders. The best model order is the one that minimizes R_{BIC}.

Lastly, the CPS includes a procedure to estimate the time scale of change T_{C} for the light curve. This value measures the length of time for which the model fit of one dataset still offers a valid description for the data included in the subsequent datasets. It is calculated by taking the residuals $\bar{\epsilon}_\iota = \bar{y}_\iota - \hat{y}_\iota(\bar{t}_\iota)$ of a dataset ι and comparing them to the residuals $\bar{\epsilon}_{\iota,\kappa} = \bar{y}_{\iota+\kappa} - \hat{y}_\iota(\bar{t}_{\iota+\kappa})$ of a later dataset $\iota + \kappa$ still calculated against the original model fit $\hat{y}_\iota$. If the residual distributions fail a two-sided Kolmogorov-Smirnov test at a significance level of $Q \geq 0.01$, the latter dataset $\iota + \kappa$ is deemed not to be described by the model fit to the original dataset ι. The time scale of change is defined to be the time interval $T_{\mathrm{C}} = \tau_{\iota+\kappa} - \tau_\iota$ between the mean epoch of the data points in the original dataset, τ_ι, and the mean epoch of the data points in the last dataset still passing the test, $\tau_{\iota+\kappa}$.

In the analysis of active star photometry, T_{C} is a candidate proxy for the spot life time on a star, as the growth and decay of the active areas cause the light curve shape to evolve. In practice, it has proved to have limited value in estimating the physical spot life times (Lehtinen et al., 2016, hereafter Paper V). Instead we find that T_{C} is sensitive to the length of the datasets. If $\Delta T_{\max}$ is increased, T_{C} will likewise increase. This shows that as the datasets get longer the light curve of the observed star has more time to evolve and smear out finer details. When the details are lost, the light curve models tend to get simpler and consequently better describe future data. Increased data precision will have an opposite effect, and we see from high precision space based photometry that the light curve profiles of the spotted stars change visibly even from one rotation to the next (e.g. Croll et al., 2006). Nevertheless, T_{C} is a useful parameter for evaluating the lengths chosen for the datasets. If the dataset lengths increase over T_{C}, it has to be concluded that the light curve has time to evolve within the individual datasets and this deteriorates the quality of the model fits. In such cases it is preferable to decrease $\Delta T_{\max}$.

Example light curve fits from the CPS for the star PW And are displayed in Fig. 4.1. The plots clearly show how the light curve shape changes between the datasets and how the fits adapt to these changes. Only the datasets labelled as independent are shown in the plot together with their mean epochs τ in years and running numbers according to the segment and dataset division. The segment division corresponds to continuous observing seasons while the datasets are numbered starting from the first dataset in each segment.

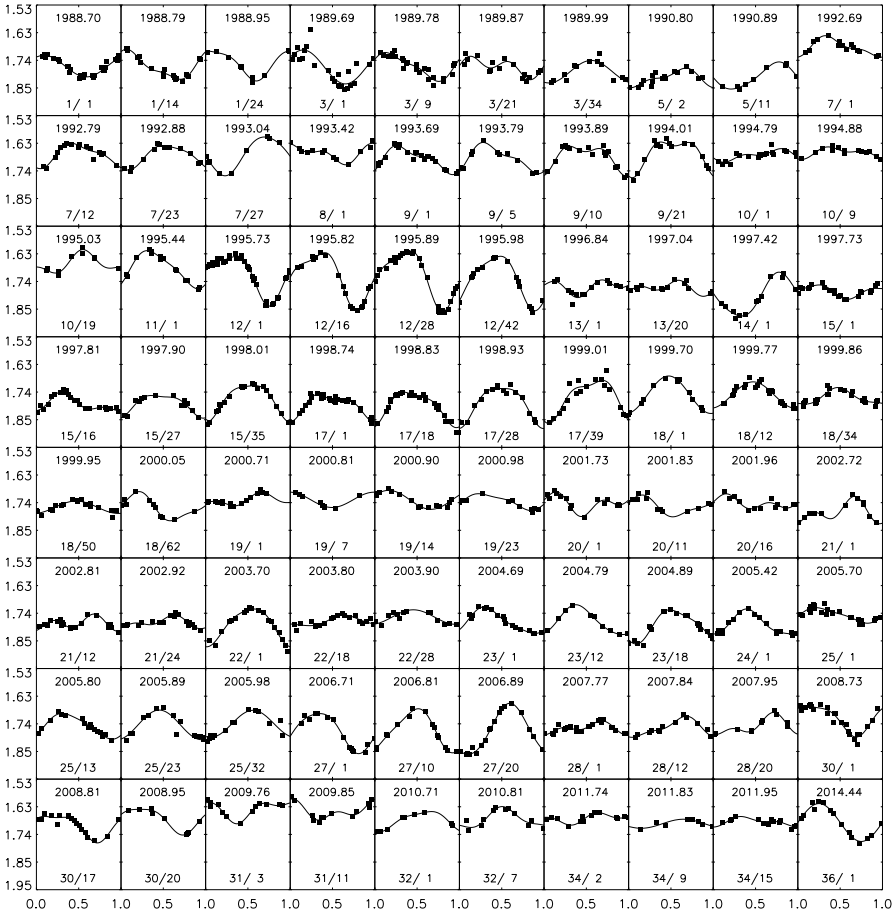

Figure 4.1: CPS fits for the independent datasets of PW And. For each dataset, the mean epoch τ is given in years above the fit and the segment/dataset numbers below the fit.

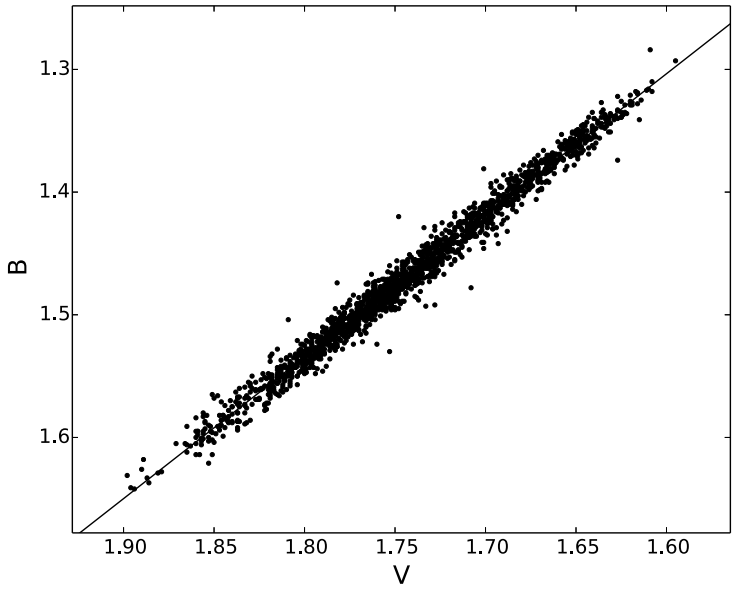

Figure 4.2: The correlation of coeval raw differential magnitudes in Johnson B and V bands from the photometry of PW And. The fit shows the linear correlation between the two colour bands.

Both the TSPA and CPS methods are formulated to be used for a single set of data at a time. However, it is possible to combine photometry from more than one passband together into a composite time series in order to increase the number of available data point and produce more stable light curve fits. One approach to this was described by Jetsu et al. (1992), were photometry from multiple passbands was transformed into a uniform normalized system. As can be seen from Fig. 4.2, there is a linear correlation between the B and V band photometry of active stars. This means that both of the bands contain essentially the same information and can be used together simply by scaling them into a common system. In Paper V we used this approach to transfer the B band photometry of our target stars into the system of the V band. This was done by finding the linear dependence between the B and V bands (see Fig. 4.2) and using this to transform the B band magnitudes into corresponding V band magnitudes. The process increased the quality of the light curve fits, but retained the reported light curve means M and amplitudes A in the system of the observed V band photometry.

4.3 Carrier Fit method

A somewhat different approach on modelling gradually evolving periodic data with a harmonic model is implemented in the Carrier Fit method (CF; Pelt et al., 2011). This method takes the same harmonic model (Eq. 4.1) as the TSPA and CPS, but allows the linear model parameters to vary themselves as functions of time; $M = M(t)$, $B_k = B_k(t)$, and $C_k = C_k(t)$. As a result, even long stretches of evolving data can be modelled in a single piece without the finer dataset division that is needed for the

TSPA and CPS.

In the CF method, all the variability in the shape of the periodic data is modelled by the time evolution of the linear model parameters. These are also responsible for modelling the period variations occurring in the data. The harmonic model itself uses only one constant frequency, $f = f_0$, which works as a modulated carrier wave. The carrier wave frequency f_0 represents the average periodicity modelled in the data.

There are two ways to model the modulation of the linear model parameters. They can be described either using splines or low frequency harmonic models similar to the main model. In Olspert et al. (2015, hereafter Paper IV) the harmonic approach was used and each of the modulated parameters $B_k^{\mathrm{CF}}(t) \in [M(t), B_k(t), C_k(t)]$ was modelled as

$$B_k^{\mathrm{CF}}(t) = C_0^B + \sum_{l=1}^{L} \left[C_l^B \cos\left(l 2\pi f_D t\right) + S_l^B \sin\left(l 2\pi f_D t\right) \right], \tag{4.9}$$

where L is the total number of harmonics in the modulator models and $f_D = D^{-1} = [C \cdot (\min(t) - \max(t))]^{-1}$ the modulator frequency calculated from the data period D. The data period has to be significantly longer than the carrier wave period $P_0 = f_0^{-1}$ in order to not disrupt the carrier wave. It has to be preferably also somewhat longer than the full range of the data, $\min(t) - \max(t)$, to allow good modelling of slow trends. In Paper IV this was achieved using a coverage factor $C = 1.2$.

Optimal values for the model and modulator function orders K and L are determined in the CF method similarly to the CPS by using the BIC. Here K and L have to minimize

$$R_{\mathrm{BIC}} = n \ln \sigma_\epsilon^2 + [(2 + 4L)K + 2L + 1] \ln n, \tag{4.10}$$

with $\sigma_\epsilon^2 = (n-1)^{-1} \sum_{i=1}^{n} \epsilon_i^2$. This searches simultaneously the optimal values of both K and L. In addition, there is an upper limit for reasonable values of L imposed by avoiding cycle count mismatches between the frequencies $f_0 - f_D$ and $f_0 + f_D$ and the resulting loss of interpolation power during extended gaps in the data. If Δ_{gap} is the length of the longest gap in the data, this means requiring $(f_0 + f_D)\Delta_{\mathrm{gap}} - (f_0 - f_D)\Delta_{\mathrm{gap}} < 1$. By taking the frequency of the highest harmonic modulator component, $f_D = L/D$, this leads to the additional condition

$$L < \frac{C \cdot (\min(t) - \max(t))}{2\Delta_{\mathrm{gap}}}. \tag{4.11}$$

The model fitting procedure in the CF method does not in itself search for the carrier frequency f_0 and this has to be found by using an auxiliary method. A powerful method for finding the carrier frequency is the phase dispersion periodogram, which is formulated in an analogous way to the Pilot Search periodogram in the TSPA (Eq. 4.2). When the correct carrier frequency f_0 has been found and the optimal values for K, L, and C have been determined, the model fit is itself computed by maximizing its goodness of fit,

$$R^2 = 1 - \frac{\sum_{i=1}^{n} (y_i - \hat{y}(t_i))^2}{\sum_{i=1}^{n} (y_i - \langle y_i \rangle)^2}. \tag{4.12}$$

In an actual analysis case of active star photometry, both the CPS and the CF methods turn out to produce very closely the same results for the light curve mean M and amplitude A and the minimum epochs $t_{\min}$ (eg. Hackman et al., 2013; Paper IV). The CF results behave like running averages of the CPS results. Depending on the exact situation, this may either mean that there is more scatter in the CPS output or

that the smooth modulation used in the CF algorithm leads to the loss of short time scale detail in its model fit. Nevertheless, both methods produce consistent results, proving that they work well in real life applications.

The nature of the CF method as a more global fit means that it can produce interpolations over longer gaps in the data or sections with poor data coverage, inaccessible to the more instantaneous fits of the CPS. This is particularly valuable when comparing results from separate observing campaigns, such as photometric analysis and DI, which all too often do not overlap with each other. On the other hand, the localized fits of the CPS provide a much easier selection of a statistically independent sample of time evolution of the model parameters. This makes its results better suited for further statistical analyses, most notably when analysing activity cycles and active longitudes.

4.4 The Horne-Baliunas method

The Lomb-Scargle periodogram has been frequently used in studies of stellar activity cycles. It is well known both from observation of the Sun and other active stars that the activity cycles are usually a quasiperiodic phenomenon and can follow a complex profile. On the other hand, the changing shape of the activity variations means that we cannot trust to use specific complex models either to provide a basis for reliable period analysis. Thus, the simple sinusoid model of the Lomb-Scargle periodogram offers a useful tool for finding periodic components in the activity data when the use of a more complex model cannot be justified.

The formulation of the periodogram by Horne & Baliunas (1986) takes the standard Lomb-Scargle periodogram

$$P_{\mathrm{LS}}(f) = \frac{1}{2}\left[\frac{\left[\sum_{i=1}^{n} y_i \cos\left(2\pi f(t_i-\tau)\right)\right]^2}{\sum_{i=1}^{n}\cos^2\left(2\pi f(t_i-\tau)\right)} + \frac{\left[\sum_{i=1}^{n} y_i \sin\left(2\pi f(t_i-\tau)\right)\right]^2}{\sum_{i=1}^{n}\sin^2\left(2\pi f(t_i-\tau)\right)}\right] \tag{4.13}$$

for the data y_i, where τ is defined by

$$\tan(4\pi f\tau) = \frac{\sum_{i=1}^{n}\sin(4\pi f t_i)}{\sum_{i=1}^{n}\cos(4\pi f t_i)}. \tag{4.14}$$

The periodogram is defined so that if the data is purely noise, the value of $P_{\mathrm{LS}}(f)$ follows an exponential distribution. Horne & Baliunas (1986) demonstrated that if the periodogram is normalized with the total variance of the data,

$$P_{\mathrm{HB}}(f) = \frac{P_{\mathrm{LS}}(f)}{\sigma^2}, \tag{4.15}$$

the distribution of the periodogram stays invariant under noise. The probability that the value of $P_{\mathrm{HB}}(f)$ at a single frequency f reaches a level higher than some observed level z is then $\Pr[P_{\mathrm{HB}}(f) > z] = \mathrm{e}^{-z}$. This behaviour allows the use of the periodogram as a statistical test for the presence of a periodic signal in the data. The critical level of the test is given by

$$Q_{\mathrm{HB}} = 1 - (1 - \mathrm{e}^{-z})^m. \tag{4.16}$$

This is also commonly called the false alarm probability, since it measures the probability that a peak of the height z or higher is observed in the periodogram purely due

to random noise. Here m is the number of independent frequencies in the periodogram, determined from numerical simulations to be

$$m = -6.362 + 1.193\,n + 0.00098\,n^2. \tag{4.17}$$

The fact that the Lomb-Scargle periodogram is often not well suited for periodic data with a complex profile, was demonstrated in Paper III for the photometry of V352 CMa. In the paper, the photometry was subjected to period analysis both using the CPS and the Horne-Baliunas method and the periods found by the two methods for the individual datasets were compared. In the case of datasets with a $K = 1$ order CPS fit, the period found in the Lomb-Scargle periodogram fell into the $\pm\sigma_P$ interval around the CPS period estimate 83% of the times. In the datasets where the CPS model order was $K = 2$, such agreement between the period estimates only happened 23% of the times. The model curve fits for the star show that in the majority of the cases of $K = 2$ models, the light curve had actually had two separate minima within the rotation period of the star. In these cases the Horne-Baliunas method, relying on the simple sinusoid model, was mislead due to being incompatible with the data.

4.5 Kuiper test

The epochs of the primary and secondary light curve minima, $t_{\mathrm{min},1}$ and $t_{\mathrm{min},2}$, offer a way to study the presence of active longitudes on an active star, since they describe the central meridian crossing times of the major spot areas. If the spot activity is concentrated on a few longitudes, the light curve minima should be located around the corresponding rotational phases.

Searching periodicity in such a series of time points requires a different approach than the study of regular time series data like light curves. One such method is the Kuiper test (Kuiper, 1960; Jetsu & Pelt, 1996) which searches for a departure from a uniform phase distribution of the time points when folded with a test frequency f. For each frequency in a search grid, the time points t_i are folded into phases ϕ_i and the phases are sorted in their rank order. Their empirical cumulative distribution on the interval $[0, 1)$ is then formed as

$$F_n(\phi) = \begin{cases} 0\,, & \phi < \phi_1 \\ in^{-1}\,, & \phi_i \le \phi < \phi_{i+1},\ 1 \le i \le n-1 \\ 1\,, & \phi \ge \phi_n. \end{cases} \tag{4.18}$$

The $F_n(\phi)$ is compared to a uniform cumulative distribution $F(\phi) = \phi$ in a way similar to the Kolmogorov-Smirnov test. The Kuiper test statistic is defined as

$$V_n = D^+ + D^-, \tag{4.19}$$

where D^+ and D^- denote the maximum values of $F_n(\phi) - F(\phi)$ and $F(\phi) - F_n(\phi)$ respectively, i.e. the greatest departures of $F_n(\phi)$ above and below $F(\phi)$. Calculating V_n for a grid of test frequencies f produces then a periodogram $V_n(f)$ which lends itself for the purpose of period search. The method assumes these periods to correspond to quasi-rigidly rotating structures. This is a fair starting assumption for active longitudes if we are not able to justify the parametrization of more complex non-rigidly rotating structures, that could be searched from the data.

Kuiper (1960) showed that the distribution of the test statistic is independent of the exact choice of $F(\phi)$ and the epoch of the zero phase. He also derived the probability

that $n^{1/2}V_n$ reaches a value as high or higher than some observed level z for phases distributed according to the reference distribution $F(\phi)$, $\Pr[n^{1/2}V_n \geq z] = P_n(z)$. The value of $P_n(z)$ is in general computable as an approximating series expansion (Jetsu & Pelt, 1996, Eq. 22). The resulting critical level of the Kuiper test for m independent test frequencies is then

$$Q_{\rm K} = 1 - (1 - P_n(z))^m. \tag{4.20}$$

4.6 Finding the correct period

Finding the correct period in the periodogram can sometimes be tricky. A problematic feature of the ground based astronomical observations is that they are limited by the observing conditions and the visibility of the target. Hence, astronomical time series typically include gaps and, in the case of nightly observations, have an approximate sampling period $P_{\rm s}$ close to one sidereal day.

The regular spacing of the observations will lead to aliasing and can cause serious issues if the underlying periodicity in the data is close to the sampling period. The resulting spurious periods can be related to the window period due to the sampling and the underlying period in the data, if it is known (Tanner, 1948). In the scheme of the light curve modelling, it is also possible to investigate the correlations of phase residuals between the data and a particular light curve model to estimate if the period is real or a spurious one (see Jetsu & Pelt, 1999, Figs. 1q–u).

In practice, the sampling of astronomical time series is rarely completely regular. Realistic observing conditions and scheduling constraints mean that the targets cannot always be monitored at the same sidereal time, such as when they reach the minimum air mass. Scatter of the observing times in the order of a few hours to one direction or the other around the optimal time is commonly the case. This non-uniformity of the sampling has useful consequences for the period analysis and the identification of the correct period. It lifts the actual Nyquist frequency, which sets the high frequency limit for frequency detection, from the value $f_{\rm Ny} = (2P_{\rm s})^{-1}$, associated with regular sampling, to a far higher value which is connected to the greatest common divisors between the time point intervals (Eyer & Bartholdi, 1999). This lies commonly considerably beyond the frequency range under investigation.

The effect of uneven sampling to the Grid Search least squares periodogram (Eq. 4.5) is illustrated in Fig. 4.3. Here sinusoidal test data was generated to mimic the photometry of PW And by setting its period at 1.75 d, amplitude at 0.1 mag, and adding Gaussian random noise with a standard deviation of 0.004 mag to the data points. Two sets of data were constructed for the test, each containing 30 data points. In one of the sets the sampling of the data is completely regular with a spacing of 1 d. The other one uses actual observing times taken from the observing record of the star. These times also have an average spacing very close to 1 d but with a certain amount of scatter around this regular pattern.

The upper panel of the plot shows the periodogram for the data with regular sampling. There are a number of identical looking minima visible in the periodogram and it is not evident which one of them corresponds to the true periodicity. The true frequency at $f \approx 0.57$ d^{-1} actually lies above the Nyquist frequency $f_{\rm Ny} = 0.5$ d^{-1} of the regular sampling and it would not be the first guess for the true periodicity in an actual analysis. In the lower panel the same analysis is done for the slightly unevenly spaced data. The aliasing frequencies are still visible in the periodogram but now they all have shallower minima than in the evenly spaced case. The uneven sampling intro-

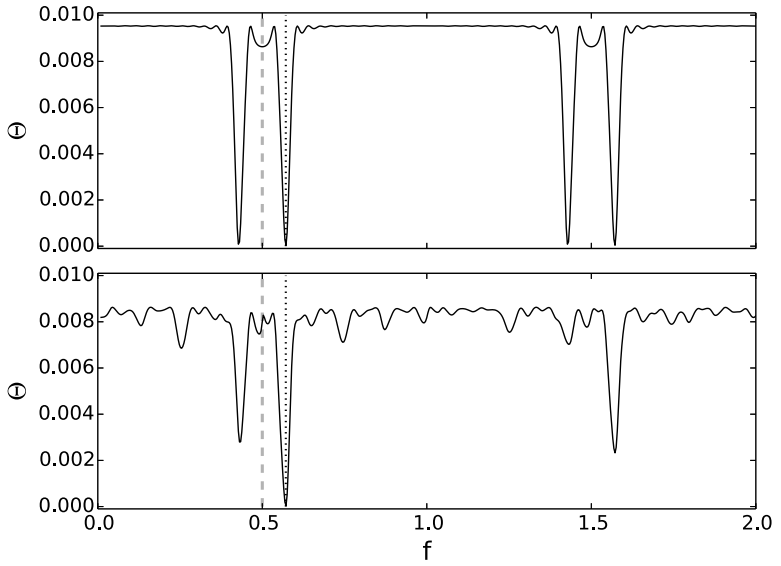

Figure 4.3: Least squares periodograms of sinusoidal data with regular sampling (*top*) and realistic uneven sampling (*bottom*). The real underlying frequency of the data is marked with the black dotted line and the Nyquist frequency for the even sampling with the grey dashed line.

duces mixing into the phasing of the data points, thus disrupting the aliasing. The only frequency unaffected by this mixing is the true underlying frequency at $f \approx 0.57$ d^{-1}. Thus, introducing a certain amount of scatter into the sampling procedure helps to downplay the effects of aliasing and aids in the identification of the true periodicity.

Moreover, knowing some physical characteristics of the target object is helpful for ruling out some unrealistic period candidates. In the case of active star photometry, the correct period has to be consistent with the stellar rotation. If there is a spectroscopic determination of the projected rotational velocity $v \sin i$ of the star, the true rotation period has to fulfil

$$P \leq \frac{2\pi R}{v \sin i}, \tag{4.21}$$

where R is the stellar radius and i the inclination of its rotation axis. The radius of a star is, of course, difficult to observe directly, but it can be estimated for example by comparing the star to theoretical stellar structure models at the same spectral type or by using the Barnes-Evans relation (Barnes et al., 1978).

5 Activity of young solar-type stars

The target sample chosen for this study consists of 21 young solar-type stars in the solar neighbourhood. They are all single stars, with no detected close stellar mass companions, and have ages estimated to range from a few million to about half a billion years. Basic properties of the stars are listed in Table 5.1, where the distances and the average magnitudes and colours are from the Hipparcos and Tycho catalogues (ESA, 1997) and the sources for the cited spectral types are given after each star. The stars are plotted in a colour-magnitude diagram in Fig. 5.1, where the zero age main sequence is indicated as the grey line according to Cox (2000). More detailed descriptions of the stellar properties can be found in Paper V.

The stars all belong to the T3 APT monitoring campaign and have mostly been chosen from the sample of solar analogues studied by Gaidos (1998). These stars have been observed continuously since 1998 or 1999. A number of additional very active solar-type stars have been part of the monitoring programme for a longer time and have been added to the observing schedule between 1987 and 1994. The only star in our sample not having a practically uninterrupted observing record is V383 Lac, which was observed from 1994 to 1996 and again from 2011 until the present.

The photometric time series analysis and the complementary determination of the chromospheric emission levels focuses on activity cycles, differential rotation, and active longitudes of the stars. Special attention is given to the description of the results to LQ Hya and NQ UMa to illustrate certain important phenomena of the stellar spot activity in more detail.

5.1 Activity cycles and trends

Right from the raw photometric observations it is evident that the changing level of spottedness causes variations in the mean brightness of the active stars on time scales from a few years up to decades (see Figs. 3.1 and 3.2). Similar variability is also seen in the chromospheric Ca II H&K time series (Baliunas et al., 1995). The commonly observed quasiperiodic nature of these variations is indicative of activity cycles seen in both photospheric spots and the chromospheres of the stars.

In the photometric results the quasiperiodic variability becomes most evident in the modelled light curve mean magnitudes, M, which we get from the CPS analysis (see Fig. 5.2). The CPS analysis also provides estimates for the light curve amplitudes, A, which likewise often show quasiperiodic patterns. A spot cycle might be expected to affect both the mean magnitude M and the light curve amplitude A of a star, reflecting the mean spottedness and the level of non-axisymmetry in the spot distribution, respectively. A full search of spot cycles should also include the composite proxies $M - A/2$ and $M + A/2$ which reflect the evolution of the minimum and maximum spotted area on the visible disk of the star (Rodonò et al., 2000).

In the full search of spot cycles from our stellar sample in Paper V, we found significant cycles in 18 of the 21 stars, using the Horne-Baliunas method (see Sect. 4.4).

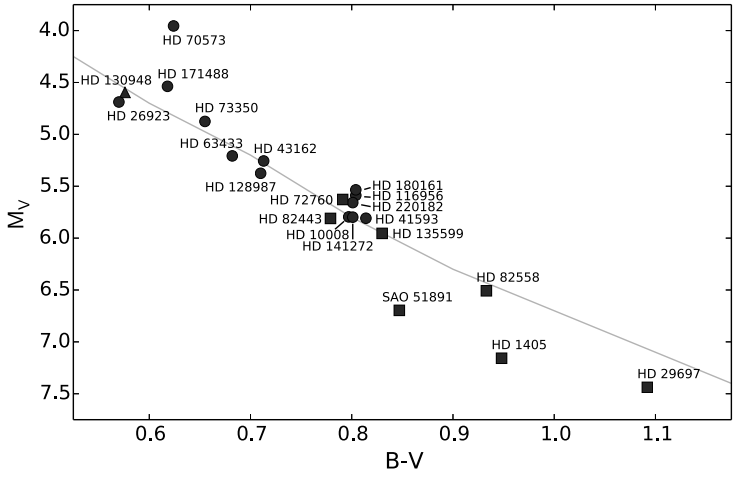

Figure 5.1: Colour magnitude diagram of the sample stars with spectral types indicated with the plot symbols: *triangle* for F, *circle* for G, and *square* for K. (Adapted from Paper V)

Table 5.1: Representative V band magnitudes, $B-V$ colours, distances, and spectral types of the sample stars.

Star	HD/SAO	V	$B-V$	d [pc]	sp.
PW And	HD 1405	8.86	0.95	21.9	K2V (Montes et al., 2001)
EX Cet	HD 10008	7.66	0.80	23.6	G9V (Gray et al., 2003)
V774 Tau	HD 26923	6.32	0.57	21.2	G0V (Gray et al., 2006)
V834 Tau	HD 29697	8.09	1.09	13.5	K4V (Gray et al., 2003)
V1386 Ori	HD 41593	6.76	0.81	15.5	G9V (Gray et al., 2003)
V352 CMa	HD 43162	6.37	0.71	16.7	G6.5V (Gray et al., 2006)
V377 Gem	HD 63433	6.90	0.68	21.8	G5V (Gray et al., 2003)
V478 Hya	HD 70573	8.69	0.62	88.5	G6V (Montes et al., 2001)
...	HD 72760	7.32	0.79	21.8	K0-V (Gray et al., 2003)
V401 Hya	HD 73350	6.74	0.66	23.6	G5V (Gray et al., 2003)
DX Leo	HD 82443	7.05	0.78	17.7	K1V (Gray et al., 2006)
LQ Hya	HD 82558	7.82	0.93	18.3	K0V (Montes et al., 2001)
NQ UMa	HD 116956	7.29	0.80	21.9	G9V (Gray et al., 2003)
KU Lib	HD 128987	7.24	0.71	23.6	G8V (Gray et al., 2006)
HP Boo	HD 130948	5.86	0.58	17.9	F9IV-V (Gray et al., 2001)
V379 Ser	HD 135599	6.92	0.83	15.6	K0V (Gaidos et al., 2000)
V382 Ser	HD 141272	7.44	0.80	21.3	G9V (Gray et al., 2003)
V889 Her	HD 171488	7.39	0.62	37.2	G2V (Montes et al., 2001)
MV Dra	HD 180161	7.04	0.80	20.0	G8V (Montes et al., 2001)
V453 And	HD 220182	7.36	0.80	21.9	G9V (Gray et al., 2003)
V383 Lac	SAO 51891	8.57	0.85	23.7	K1V (Montes et al., 2001)

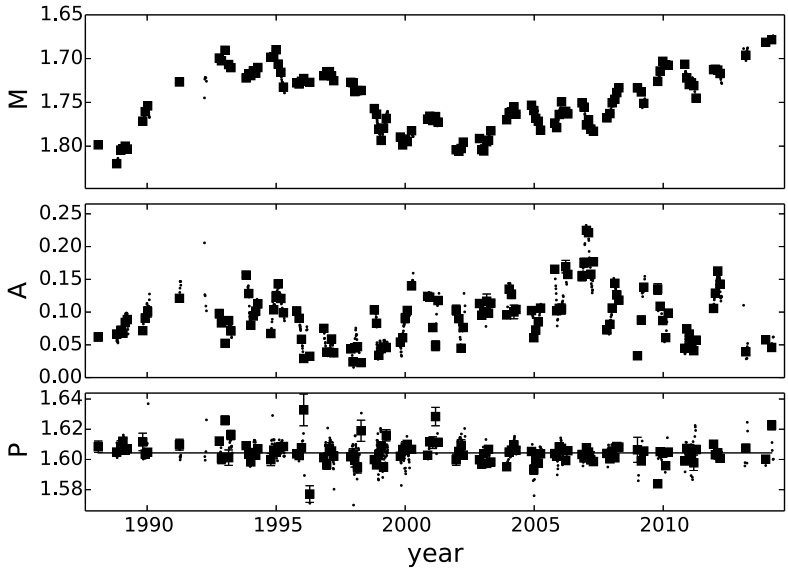

Figure 5.2: M, A, and P results from the CPS analysis of LQ Hya. Estimates from the independent datasets are shown with squares and the weighted mean period $P_{\rm w}$ with the horizontal line over the P estimates. (Adapted from Paper V)

The criterion for finding a cycle in the data was that there would be a periodic signal with $Q_{\rm HB} \leq 0.1$ in at least one of the proxies M, A, $M-A/2$, or $M+A/2$. Additionally, following the cycle classification of Baliunas et al. (1995), we graded the cycles reaching only $0.01 < Q_{\rm HB} \leq 0.1$ as "poor". Only five out of the 18 star showing cyclicity had just a "poor" cycle. Moreover, no cycles were found on the star V383 Lac simply because its photometric record is patchy and therefore it had to be excluded from the cycle search. However, the mean magnitude of V383 Lac shows exceedingly large variability between the beginning and the end of the observing record, implying that it probably also has a prominent spot cycle. It can thus be concluded that the spot cycles are a common or even a nearly universal phenomenon in the young active solar type stars.

Most of the stars in the sample show only a single cycle but in a few cases two simultaneous cycles with different periods can be identified. On V377 Gem there are cycles of 2.67 ± 0.02 yr and 8.0 ± 0.2 yr, on DX Leo cycles of 4.12 ± 0.03 yr and 20.0 ± 0.7 yr, and on NQ UMa cycles of 2.93 ± 0.02 yr and 14.7 ± 0.5 yr. The ratios between the long and short cycles are respectively 3.0, 4.9, and 5.0. On DX Leo and NQ UMa the cycle period ratios are quite close to each other and the ratio on V377 Gem is not terribly far from them either. This observation is suggestive of a universal relation between two superimposed cycles. Moreover, a short cycle with a period around 3 yr has been reported for LQ Hya by a number of authors (eg. Oláh et al., 2009). If this is compared to our estimates of the long cycle period ranging between 14.5 ± 0.3 yr and 18.0 ± 0.2 yr, we find a period ratio between 5 and 6, again supporting a general relation between the short and long cycle periods. The short cycle on LQ Hya is also suggested by our data (Lehtinen et al., 2012, hereafter Paper II) but ultimately the

Horne-Baliunas method was incapable of detecting it.

LQ Hya also provides an example of how non-stationary the activity cycles can be. There is strong variability in the CPS results of the star seen in both the M and the A data (see Fig. 5.2). Indeed, a highly significant long cycle period is found in both of them as well as in $M - A/2$ and $M + A/2$. There is noticeable variation, however, in the period values and none of the tested proxies produce exactly comparable results. The detected cycle period values are 17.4 ± 0.2 yr for M, 14.5 ± 0.3 yr for A, 15.8 ± 0.2 yr for $M - A/2$, and 18.0 ± 0.2 yr for $M + A/2$. These period values are too close to each other to be considered separate cycles but still too widely dispersed for a stable mean period to be identified. Moreover, the naive error estimates of cycle periods clearly underestimate the full uncertainty present in the period estimation. Hence, the cycle period errors, calculated assuming stationary periodicity, have to be considered unreliable. Even more significantly, looking at older data (e.g. Jetsu, 1993) reveals that there was a brightness maximum around 1985, just before the brightness minimum seen in our data in 1989 and merely six years before the mean brightness reaching its maximum level again in 1991. This explains the cycle period values of around 6 yr published by a number of authors (e.g. Jetsu, 1993; Kővári et al., 2004) as well as the changing cycle length from 7 yr to 12.4 yr reported by Oláh et al. (2009), and further demonstrates the poor cycle stability.

Quasiperiodic variability is by far most commonly found in the M results, $M - A/2$ and $M + A/2$ being the next common proxies to show cyclicity. In total, 16 of the identified cycles were found at least in M. The least common proxy to show cyclicity was A, with only seven identified cases. This implies that the quasiperiodic activity variations are more likely to impact the mean level of spottedness than the axisymmetry of the spot distribution. A similar case is observed on the Sun where the 11 year spot cycle is observed specifically in the sunspot number. However, three of the identified cycles appear only in the A data, suggesting that pure modulation of axisymmetry alone is also an alternative for a spot cycle.

Compared to the mean brightness, M, and the light curve amplitude, A, the light curve period, P, shows a distinct lack of systematic variability for all of the stars. On the Sun sunspots are formed on average closer to the poles at the start of each spot cycle and their formation latitudes drift closer to the equator as an activity wave during the course of the cycle. Surface differential rotation on the Sun causes the spots closer to the equator to follow a faster rotation period than spots closer to the poles, which imposes a systematic change in the mean rotation period of the spots over a whole activity cycle. The fact that we do not see anything like this in the CPS results of our stars suggests that there may not be such latitudinal activity waves on these stars, or at least that their impact on the observed rotation periods is drowned by other factors affecting the period estimation. Even on the Sun there is a lot of scatter in the actual rotation periods observed on the sunspots and the differential rotation law is not particularly evident in the data (Howard, 1994, Fig. 2).

More systematic comparison of the cycle periods can be achieved by following the procedure of Brandenburg et al. (1998) and Saar & Brandenburg (1999). They compared the ratio of the cycle and rotation periods $P_{\rm rot}/P_{\rm cyc}$ to the inverse Rossby number, defined to be equal to the Coriolis number $\mathrm{Ro}^{-1} = \mathrm{Co} = 2\Omega\tau_c = 4\pi\tau_c/P_{\rm rot}$, to search for systematics in the cycle periods observed on active stars with different rotation rates. This comparison involves calculating the convective turnover time τ_c for which we used the semi-empirical formula given by Noyes et al. (1984). This formula allows the estimation of τ_c as a function of the $B - V$ colour of a star.

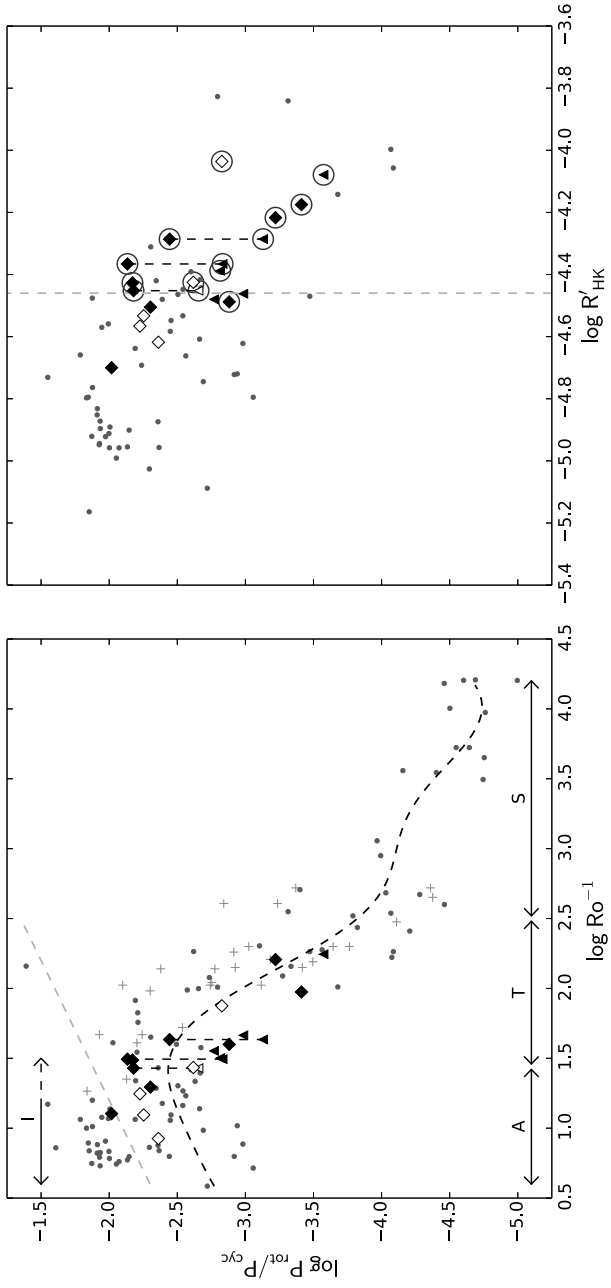

Figure 5.3: *Left:* $\log P_{\rm rot}/P_{\rm cyc}$ vs. $\log {\rm Ro}^{-1}$. Our stars are marked with the diamonds, which are white for cycles graded "poor" and black otherwise. Reference data is shown from Saar & Brandenburg (1999) (*grey points*) and Oláh et al. (2000, 2009) (*grey pluses*). The rough $\log {\rm Ro}^{-1}$ ranges of the activity branches are marked by arrows and labelled "I" for "Inactive", "A" for "Active", "T" for "Transitional", and "S" for "Superactive" *Right:* Same as on the left but for $\log P_{\rm rot}/P_{\rm cyc}$ vs. $\log R'_{\rm HK}$. Those of our stars with detected active longitudes have their symbols circled. (Adapted from Paper V)

The comparison of $P_{\rm rot}/P_{\rm cyc}$ to Ro^{-1} has theoretical advantages but it suffers from the fact that τ_c cannot be observed directly. The Rossby number is also itself a function of the stellar rotation period so inherent spurious correlation is expected between it and $P_{\rm rot}/P_{\rm cyc}$, even if these values would be physically unrelated to each other. Both of these problems can be solved by performing a second comparison between $P_{\rm rot}/P_{\rm cyc}$ and $\log R'_{\rm HK}$, as there is a one-to-one connection between Ro^{-1} and the activity level of a star, as measured by chromospheric emission (Noyes et al., 1984). The emission index $\log R'_{\rm HK}$ is ideally suited for the task since it is easy to observe directly and its value is statistically as well as observationally fully independent of $P_{\rm rot}/P_{\rm cyc}$, allowing the elimination of spurious correlations.

The comparisons of $\log P_{\rm rot}/P_{\rm cyc}$ vs. $\log \mathrm{Ro}^{-1}$ and $\log P_{\rm rot}/P_{\rm cyc}$ vs. $\log R'_{\rm HK}$ are shown in Fig. 5.3 for our stars and a set of reference stars taken from Saar & Brandenburg (1999) (*grey points*) and Oláh et al. (2000, 2009) and references therein (*grey pluses*). In both cases our results line up with the previously published results and the same structures can be seen in the distribution of $\log P_{\rm rot}/P_{\rm cyc}$ both against $\log \mathrm{Ro}^{-1}$ and $\log R'_{\rm HK}$. The stars fall on a sequence of distinct activity branches that range from modest activity on the left edges of the plots to extremely strong activity on the right edges. The branches are labelled following Saar & Brandenburg (1999) as "Inactive", "Active", "Transitional", and "Superactive". In the left panel of Fig. 5.3, their approximate extents in $\log \mathrm{Ro}^{-1}$ are shown by the arrows labelled "I", "A", "T", and "S" and a rough division between the "Active" and "Inactive" branches is marked by the light grey dashed line. These are all rough borders since the currently available data allows little more than a visual identification of the branches.

The stars in our sample, with one exception, fall on the "Active" and "Transitional" branches and show that there is a continuous transition between them. This is in contrast to the relation between the "Active" and "Inactive" branches which appear as discontinuous or parallel to each other. A smooth adaptive Gaussian process fit (Haran, 2011) to the "Active" – "Transitional" – "Superactive" sequence in the data from Saar & Brandenburg (1999) and Paper V is shown as the curved black dashed line. It traces this sequence from the least active stars to the most active ones and its maximum is located at the position where the junction between the "Active" and "Transitional" branches can be placed. In the Gaussian process fit the location of this turnoff point is at $\log \mathrm{Ro}^{-1} = 1.42$. The activity cycle lengths appear to follow different patterns at the opposite sides of this divide, so that within the "Active" branch increasing Ro^{-1} leads to shorter fractional cycle lengths but in the "Transitional" and "Superactive" branches this turns into a clear trend towards increasing cycle lengths. The observed pattern indicates that the stellar dynamos probably experience a fundamental change near this value.

A feature that is not seen in the previously published cycle data but is evident in ours, is the split of the activity cycles into two parallel subbranches. This is particularly evident in the $\log P_{\rm rot}/P_{\rm cyc}$ vs. $\log R'_{\rm HK}$ plot. It is significant that for the three stars with double cycles (connected together with the vertical dashed lines) the two cycles fall on the separate subbranches. This verifies the suspicion of a systematic relation between the short and long cycles, evoked by the similar cycle length ratios on the different stars. Such subbranches are indicative of multiple different cycle modes that can be excited for a stellar dynamo but it is still unclear how they should be related to the previously published results. Böhm-Vitense (2007) suggested a division of the "Active" branch into two subbranches but these cannot be easily interpreted as our subbranches.

5.2 Differential rotation

As described in in Chapter 3, the range of photometric rotation periods detected on an active star can be used to estimate the magnitude of its surface differential rotation. We have estimated this period range with the relative $\pm 3\sigma$ limits following Jetsu (1993),

$$Z = \frac{6\Delta P_{\rm w}}{P_{\rm w}}. \tag{5.1}$$

Here

$$P_{\rm w} = \frac{\sum w_i P_i}{\sum w_i} \tag{5.2}$$

is the weighted mean and

$$\Delta P_{\rm w} = \sqrt{\frac{\sum w_i (P_i - P_{\rm w})^2}{\sum w_i}} \tag{5.3}$$

the weighted standard deviation of the individual period estimates P_i from the independent datasets of the CPS analysis. For the weights we have used the inverse square errors of the period estimates, $w_i = \sigma_{P,i}^{-2}$. If the period estimates were to represent the full range of surface rotation periods between the stellar equator and poles, the period range Z would be a direct estimate of the relative differential rotation coefficient, $Z \approx k = \Delta\Omega/\Omega$.

With multiple simultaneous spots on different latitudes, differential rotation can in principle also be measured from the resulting beating pattern in the light curve. Such patterns are common in the highly precise satellite photometry (e.g. Fröhlich et al., 2012). They can sometimes even be detected from the less accurate and more sparsely sampled ground based photometry (Hackman et al., 2013).

In reality, the value of Z cannot be interpreted as a measure of the differential rotation that simply. Directly equating Z to k would require the observed period range to include rotational signatures up to the stellar poles. However, the closer a spot lies to the pole, the weaker is the observed rotational modulation it causes. A spot situated symmetrically on the visible pole will not cause any modulation at all and we are thus unable to gain direct information of the polar rotation. We also know from the solar analogy and the DI results of other active stars that the spots are typically confined to narrower latitude bands instead of a full equator to pole extent. This all implies that the value of Z may underestimate the surface differential rotation coefficient.

Moreover, active region growth and decay continuously alters the observed light curve shapes, leading to additional variability in the estimated periods. Similarly, observational errors, sparse data coverage, and the requirement to use datasets of limited length to get local period estimates, introduce a spurious component to the period variations. These effects contribute to the estimated Z by inflating it from the value simply due to the differential rotation.

To estimate these additional contributions to Z, we performed numerical experiments in Paper V with CPS analysis for a set of noisy sinusoidal data having a constant period. From these we calculated an estimate for the spurious period fluctuations $Z_{\rm spu}$ that were simply due to the numerical instability introduced by the sparse and noisy data. The test results showed that $Z_{\rm spu}$ depends of the number of data points per dataset, $n_{\rm data}$, the number of complete rotations within each dataset, $n_{\rm rot}$, and the ratio of observational noise to the signal amplitude, $\epsilon = 2\sigma/A$. Our approximation was

$$Z_{\rm spu} = 16.0\, \epsilon n_{\rm rot}^{-1}(n_{\rm data}^{-1} + 0.023). \tag{5.4}$$

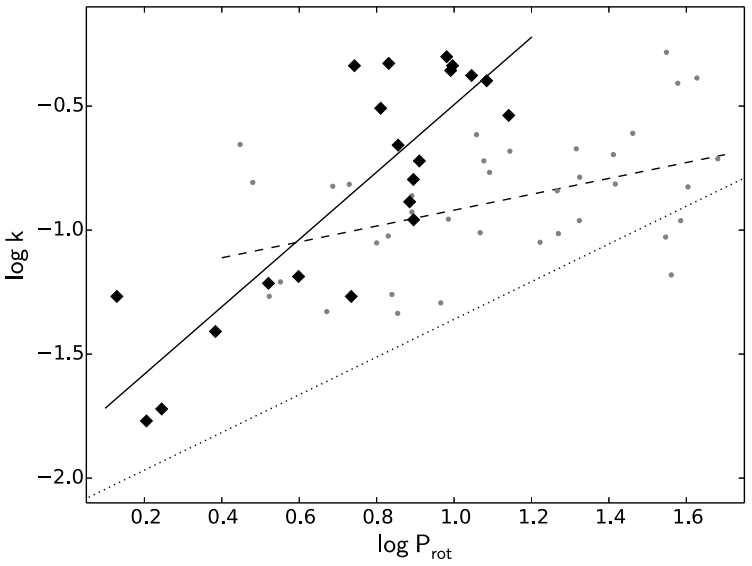

Figure 5.4: Estimated differential rotation vs. rotation period for our sample stars shown with the diamonds and the fit of Eq. 5.5 as the solid line. Comparison data from Donahue et al. (1996) is shown as gray points and their fit as the dashed line. The fit to the stars of Henry et al. (1995) is indicated as the dotted line. (Adapted from Paper V)

Using the average values for $n_{\rm data}$, $n_{\rm rot}$, and ϵ, we found that the predicted values of $Z_{\rm spu}$ for our sample stars were always in the range of a few percent of the observational Z values. Thus the Z estimates seem reasonably stable against numerical instability. There is furthermore reason to believe that within the time scale of a few rotations, similar to our dataset lengths, active region growth and decay also produces a relatively minor effect on the period fluctuations (Dobson et al., 1990). We can thus say that the uncertainty in relating the Z from the CPS analysis to k is dominated by the unknown latitude extent of the spot areas on the stars. While this method has limited power in estimating the differential rotation of individual stars, it does provide information on whether a particular star has weak or strong differential rotation. It can in particular be used as a proxy measurement of k in larger stellar samples by using the proportionality $Z \propto k$. This is a useful result in studying the general dependence of the differential rotation from other stellar parameters.

Despite all the uncertainties associated with measuring the differential rotation, there is a clear dependence between Z and the rotation period. Stars that have shorter rotation periods have smaller values of Z and thus appear to have smaller differential rotation. For our stars we find a linear relation in the logarithmic scale as

$$\log Z = -1.85 + 1.36 \log P_{\rm rot}. \tag{5.5}$$

The fit and the stars are shown in Fig. 5.4.

This relation can be compared to previous results obtained by other authors. Henry

Table 5.2: Power law indices μ and ν and their reported errors $\sigma_{\{\mu,\nu\}}$ for the differential rotation relations $k \propto P_{\rm rot}^{\mu}$ and $\Delta\Omega \propto \Omega^{\nu}$.

μ	ν	$\sigma_{\{\mu,\nu\}}$	Reference
0.76	0.24	0.06	Henry et al. (1995)
0.3	0.7	0.1	Donahue et al. (1996)
0.85	0.15	0.10	Barnes et al. (2005)
0.71	0.29	...	Reinhold & Gizon (2015)
1.36	−0.36	0.19	Paper V

et al. (1995) performed a study where they traced the rotation of light curve features identified as distinct spots. They estimated k using the difference ΔP between the largest and smallest detected periods. Combining their results to those of Hall (1991), they found

$$\log k = -2.12 + 0.76 \log P_{\rm rot} - 0.57\, F, \tag{5.6}$$

where F is the Roche lobe filling factor. Donahue et al. (1996) investigated rotational variation on active stars as seen in the Ca II H&K line emission and estimated differential rotation by finding ΔP from seasonally computed periodograms. They found a scaling law $\Delta P \propto P_{\rm rot}^{1.3}$, corresponding to scaling the differential rotation coefficient as $k \propto \Delta P/P \propto P_{\rm rot}^{0.3}$.

The relations found by Henry et al. (1995) and Donahue et al. (1996) are both shown in Fig. 5.4 in comparison to our results. Since all our stars lack close binary companions, the comparison is done by setting $F = 0$ for Eq. 5.6. There is qualitative agreement between the three results but the exact values predicted for the differential rotation deviate quite a bit between them. This can be expected to an extent since the methods used in the studies to estimate the differential rotation also differ from each other in their formulation.

Further studies were made by Reinhold et al. (2013) and Reinhold & Gizon (2015) from a periodogram analysis of Kepler photometry of a large sample of stars and by Barnes et al. (2005) based on DI results. Reinhold & Gizon (2015) reported a scaling law $k \propto P_{\rm rot}^{0.71}$, close to the results of Henry et al. (1995), after discarding the hottest stars in their sample. Barnes et al. (2005) reported the scaling of the absolute differential equator to pole shear $\Delta\Omega$ to the rotation rate Ω as $\Delta\Omega \propto \Omega^{0.15}$. This corresponds to $k \propto P_{\rm rot}^{0.85}$, which is again qualitatively similar to the other results in showing increasing differential rotation towards slower rotators. In general, we find that if we have $k \propto P_{\rm rot}^{\mu}$ for the differential rotation coefficient, we get $\Delta\Omega \propto \Omega^{\nu} = \Omega^{1-\mu}$ for the absolute shear. The power law indices μ and ν and their reported error estimates are listed for all the mentioned studies in Table 5.2.

The values of μ and ν show considerable scatter between the different studies. The differences between the exact obtained values probably originate from different choices of data analysis strategies and the physical rotation proxies being tracked, as well as simple random scatter due to limited sample sizes. In the case of our sample and that of Donahue et al. (1996) even the power law nature of the underlying scaling cannot be fully verified since they both cover only approximately one order of magnitude in $P_{\rm rot}$.

Nevertheless, at least in the case of k the results may be interpreted to qualitatively agree with each other since they show slower rotating stars to have stronger differential rotation. In the case of the dependence of $\Delta\Omega$ from Ω the results are less clear, but as they are scattered closer to $\nu = 0$, they may still suggest an agreement with theoretical

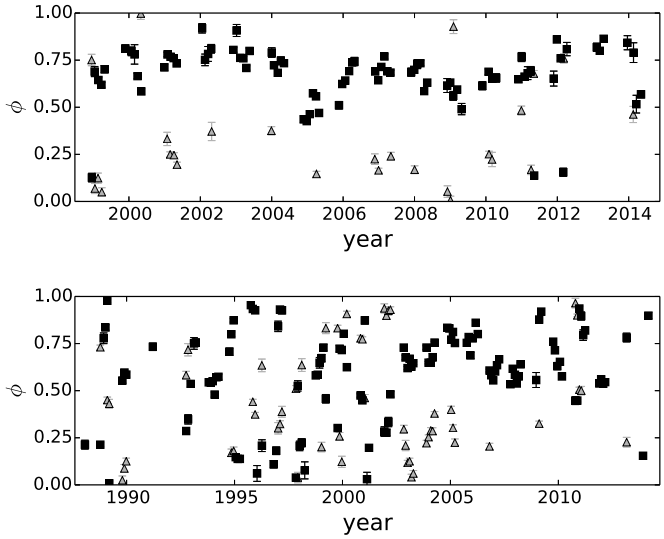

Figure 5.5: Light curve minimum phases for NQ UMa (*top*) and LQ Hya (*bottom*) showing the active longitudes on the stars. (Adapted from Paper V)

results. Küker & Rüdiger (2011), for example, found $\Delta\Omega$ to have little dependence from the rotation rate in their mean field models computed for lower main sequence stars.

According to Barnes et al. (2005) and Collier Cameron (2007) there is a strong dependence of $\Delta\Omega$ from the temperature of the star. We were unable to find evidence for this from our results in Paper V, only finding a Pearson correlation coefficient $r = -0.21$ between the $B-V$ colour and $Z/P_{\rm rot} \propto \Delta\Omega$. Our results agreed better with Küker & Rüdiger (2011) who found only weak temperature dependence of $\Delta\Omega$ for stars with temperatures within the range 3500–6000 K and a steeper dependence only for stars hotter than this. The two staged temperature dependence was also observationally seen by Reinhold et al. (2013), whose sample included stars both hotter and cooler than 6000 K.

5.3 Active longitudes and flip-flops

In the same way as activity cycles, active longitudes appear to be a common phenomenon in active stars. A total of nine stars in our sample show persistent or episodic active longitudes with the Kuiper test yielding critical levels $Q_{\rm K} < 0.01$ and two more with critical elvels $Q_{\rm K} < 0.05$ (see Sect. 4.5). Examples are shown in Fig. 5.5 for NQ UMa and LQ Hya. The active longitudes are structures where the spots, traced by the light curve minima, are grouped into more or less tightly confined ranges of rotational phase which retain their coherence for a period of several years.

As a rule, there are only one or two active longitudes visible on the stars at any given time. In our analyses we have used light curve model orders of $K \leq 2$, so no more simultaneous minima could have been detected. However, each spot, no matter how compact, produces a very broad depression into the light curve, affecting how

well distinct spots or spot areas can be resolved from each other in the photometry. The contributed minima to the light curve from spots too close to each other in the longitudinal direction will merge, and instead of producing two separate minima, a single merged minimum will be seen. It turns out that two spots of equal contribution to the light curve have to have a phase separation of about $\Delta\phi \approx 0.33$ in order to produce clearly separate minima (Paper I). As a result, three simultaneous minima are an exceedingly rare event for an active star light curve and more complex light curve shapes than that do not exist. Thus we only expect to see two active longitudes at most located roughly on the opposite sides of the stars and confining the CPS light curve fits to $K \leq 2$ models is well justified.

In between the datasets the restriction to only two simultaneously observable minima does not hinder the estimation of the full longitudinal distribution of the starspots. If there are no active longitudes on a star and the spots are formed randomly on all longitudes, the light curve minima of independent datasets close in time can be on totally different rotational phases. Over the course of time the minima will appear randomly across all the phases. Only if there is a stable active longitude structure physically present on the star, will the observed minima concentrate systematically around certain phases.

There is a variety of different active longitude structures observed on the stars. Depending on the star in question, there may be one or two active longitudes visible and the structures can either stay stable for decades and span the whole extent of the data or be more episodic, appearing in only part of the data. Quite often we also see variable short lived migration patterns where the active longitudes move back and forth at different rotation periods around their mean period. Modest migration can be seen in the active longitudes of both NQ UMa and LQ Hya (Fig. 5.5).

LQ Hya offers a case of a star where the active longitudes occur in only part of the data. The pattern found by the Kuiper test existed with a tight phase coherence from 2003 to about 2008, while another episode of phase coherence occurred before 1995. This previous active longitude pattern is tentatively suggested by the CPS results (Paper II) but can more clearly be seen in the CF analysis (Paper IV). For the rest of the observing record, no active longitudes can be identified. In fact, the search for a correct carrier wave for the CF analysis indicated that a single representative carrier wave period could only be found using correlation lengths less than about 230 days. The detailed CPS analysis for LQ Hya revealed that within each observing season, lasting about 180 days, one sees relative phase coherence in the light curve minima, but for the most part this is lost when looking at the data as a whole.

The active longitudes of NQ UMa show fairly clearly one more transient phenomenon. During the 1998–1999 observing season there was a flip-flop event where the main spot activity changed mid-season from one active longitude to the other. In the light curve this could be seen as complete flattening of the original primary minimum while at the same time the original secondary minimum grew deeper (see Paper I). Generally speaking, such flip-flop events have not been too frequent in our sample stars. The typical situation has been that the main spot activity remains on one active longitude for extended periods of time. On NQ UMa there were two smaller phase jumps in 2004 and 2014 and a slower phase shift during 2006. These were all about $\Delta\phi \approx 0.25$ in size, so whatever their correct interpretation is, they do not fit into the description of a classical flip-flop where the activity experiences a full $\Delta\phi \approx 0.5$ shift in phase (Hackman et al., 2013). Nevertheless, a concise theory to explain all the observed flip-flop like events, or fast changes in the inferred longitudes of the activity, is

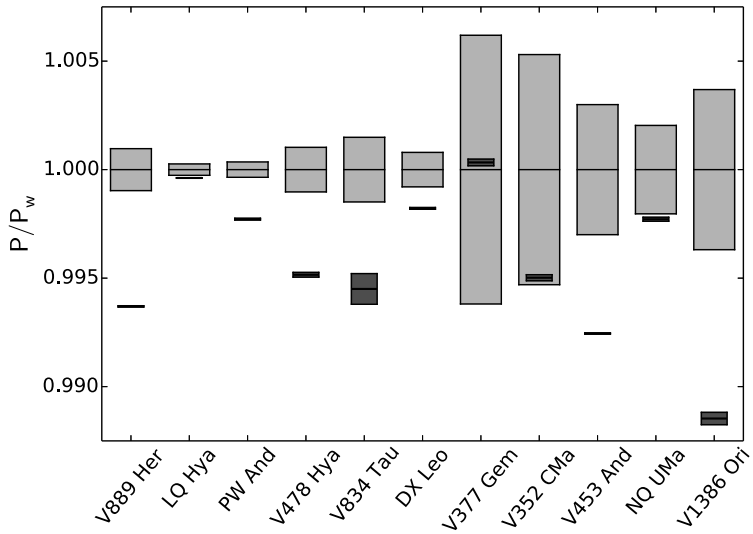

Figure 5.6: Comparison of the active longitude periods $P_{\rm al}$ (dark boxes) to the photometric mean rotation periods $P_{\rm w}$ (light boxes), both normalized to the values of $P_{\rm w}$. The heights of the boxes show the estimated $\pm 1\sigma$ error bars of the periods. (Adapted from Paper V)

still lacking, so also these smaller phase shifts need to be considered when developing models to explain flip-flops. Further flip-flop events were identified in Paper V on DX Leo between 1993 and 1994 and on PW And in 1989, 2000, and 2002. The detailed CF analysis of LQ Hya in Paper IV revealed a total of seven flip-flop like events between 1988 and 2014. All but one of these, happening in 1992, occurred during time periods when there definitely were no active longitudes present on the star. Hence, they do not fit into the strictest definition of a flip-flop, which requires the activity to be confined in stable active longitudes both before and after the phase shift (Hackman et al., 2013). A possible explanation would be that they have resulted from intermittent beating patterns caused by differential rotation. Moreover, there appears to be no repeatable evidence for the regular flip-flop cycles that have been previously suggested (Berdyugina & Tuominen, 1998; Berdyugina et al., 2002).

The Kuiper test provides both a detection method for the active longitudes as well as a way to estimate the rotation period associated to them. The active longitude period $P_{\rm al}$ is related to the physical rotation of the star, so it has to have a value close to the mean photometric rotation period, estimated as $P_{\rm w}$. However, they do not necessarily have to be identical. The photometric period tracks the rotation of the individual spots or spot areas on the stellar surface, while the active longitude period traces the rotation of the underlying magnetic structure manifesting itself as the active longitudes. If there is a difference between the rotation of this magnetic structure and the surface plasma, we expect new spots to form at the active longitudes, following $P_{\rm al}$, but then start to drift away from these longitudes following the surface rotation at $P_{\rm w}$.

Fig. 5.6 shows the photometric and active longitude rotation periods of the 11 stars where active longitudes were detected in Paper V, normalized by the photometric periods $P_{\rm w}$ of each star. On seven stars there is a significant difference between the $P_{\rm al}$ and $P_{\rm w}$ values, which is unlikely to be explained as a statistical fluke. In all these cases $P_{\rm al}$ is shorter than $P_{\rm w}$.

The observed differences between $P_{\rm al}$ and $P_{\rm w}$ can have a couple of different interpretations. It might be that the magnetic structures that sustain the active longitudes reside at deeper levels in the stellar interior than the formed starspots and trace the rotation at those depths. In this case the difference between $P_{\rm al}$ and $P_{\rm w}$ would reflect radial shear in the outer layers of the stellar interior. Helioseismological results have shown that in the Sun there is a negative gradient of angular velocity on all latitudes just below the photosphere (Howe et al., 2000). Such behaviour of internal rotation would predict shorter rotation periods for structures rooted at deeper levels, just as observed for the active longitudes on our stars.

On the other hand, there is theoretical evidence from direct numerical simulations that a stellar dynamo may operate with a non-axisymmetric mode that propagates longitudinally with respect to the rotational reference frame of the star (Cole et al., 2014). If this is the case for our stars, what we are seeing as the migrating active longitudes are signs of azimuthal dynamo waves, being the azimuthal counterpart to the latitudinal dynamo waves seen on the Sun and responsible for the well known butterfly diagram (Rädler, 1986).

Similar drift patterns have been observed before in active giants stars. Lindborg et al. (2011) observed from DI that the active longitude on II Peg has followed a shorter rotation period than the stellar surface, and the observation was reinforced by Hackman et al. (2012) who compared the DI results to photometry. An opposite pattern seems to have been present on FK Com, where the active longitudes have a slower rotation period than the stellar surface (Hackman et al., 2013).

A second significant result concerning the active longitudes is their presence on only the more active stars. This is shown on the right panel of Fig. 5.3, where the stars with active longitudes detected with $Q_{\rm K} < 0.05$ are circled. The plot does not include stars lacking activity cycle detections, but these all also lack active longitudes.

There is a sharp divide at approximately $\log R'_{\rm HK} = -4.46$ between the more active stars showing active longitudes and the less active stars with poor or no evidence for them. Only two exceptions from this rule can be seen in our data. One is V478 Hya, which has well developed active longitudes but lies just on the inactive side of the $\log R'_{\rm HK} = -4.46$ limit. The other one is V383 Lac, which has a high chromospheric activity level at $\log R'_{\rm HK} = -4.327$, but lacks detections for both active longitudes and activity cycles. The fact that the photometric record of this star is so patchy, can be the reason behind both of these non-detections. During the first three year part of the observations a phase coherent structure can indeed be seen in the light curve minima of the star (see Paper V). If more observations had been available, this structure may have turned out to be a long lived active longitude.

As a result, the sharp divide at the intermediate activity values to stars with and without active longitudes appears well defined. The two sides of the divide can be identified as two well defined domains of magnetic field geometry. Since the spots can be used as tracers of the surface magnetism, the large scale magnetic field appears to prefer an axisymmetric configuration on the less active stars, whereas on the more active stars the field configuration is dominated by a non-axisymmetric mode. This observation can be related to the numerical results of Tuominen et al. (1999) who found

their mean field dynamo solutions to switch from axisymmetric to non-axisymmetric with increasing Taylor numbers, i.e. higher rotation rates. Direct magnetic mapping of solar-like stars by ZDI also appears to suggest that faster rotating F, G, and K type active stars prefer non-axisymmetric toroidal field geometries over axisymmetric poloidal fields that are preferred by their slower rotating counterparts (Fares, 2014).

The divide is coincidentally close to the junction of the "Active" and "Transitional" activity branches seen in the cycle lengths. It is thus possible that the divide to stars with axisymmetric and non-axisymmetric field configurations is related to the mechanism responsible for the turnoff point between these two branches.

6 Summary of the publications

This thesis consists of the following five peer-reviewed journal articles. They are presented in the chronological order, which also reflects the logical progress of the study.

- **Paper I: J. Lehtinen**, L. Jetsu, T. Hackman, P. Kajatkari, and G. W. Henry, 2011, "The continuous period search method and its application to the young solar analogue HD 116956", Astronomy Astrophysics, 527, A136
- **Paper II: J. Lehtinen**, L. Jetsu, T. Hackman, P. Kajatkari, and G. W. Henry, 2012, "Spot activity of LQ Hydra from photometry between 1988 and 2011", Astronomy & Astrophysics, 542, A38
- **Paper III:** P. Kajatkari, L.Jetsu, E. Cole, T. Hackman, G. W. Henry, S.-L. Joutsiniemi, **J. Lehtinen**, V. Mäkelä, S. Porceddu, K. Ryynänen, and V. Şolea, 2015, "Periodicity in some light curves of the solar analogue V352 Canis Majoris", Astronomy & Astrophysics, 577, A84
- **Paper IV:** N. Olspert, M. J. Käpylä, J. Pelt, E. M. Cole, T. Hackman, **J. Lehtinen**, and G. W. Henry, 2015, "Multiperiodicity, modulations, and flip-flops in variable star light curves. III. Carrier fit analysis of LQ Hydrae photometry for 1982–2014", Astronomy & Astrophysics, 577, A120
- **Paper V: J. Lehtinen**, L. Jetsu, T. Hackman, P. Kajatkari, and G. W. Henry, 2016, "Activity trends in young solar-type stars", Astronomy & Astrophysics, 588, A38

The papers are summarised in the following sections and the author's contributions are specified at the end of each section.

6.1 Paper I

Paper I contains the formulation and characterization of the CPS method. In this paper we described the changes implemented to the CPS differentiating it from the TSPA method, i.e. the automated selection of short datasets from the time series data using a sliding window, the selection of the order for the harmonic model using the BIC, and the calculation of the time scale of change for the model fits.

We performed three tests with artificial data to characterize the performance of the CPS with different kinds of input data. The first test investigated how well the BIC performs in choosing the model order. We used the CPS to analyze data generated with harmonic models of the orders, $K = 0$, $K = 1$, and $K = 2$ and with different ratios of signal amplitude to noise. In the case of periodic data, the correct model order was selected with a decent success rate in all of the test cases. With non-periodic data we found an elevated rate of spuriously detected periodicity, especially in the case of datasets with low numbers of data points. Attention should be paid to this when

applying the CPS, so that the spuriously detected periods do not interfere with the overall quality of the time series analysis. In the second test we applied the CPS to a time series with two equally deep minima slowly diverging from each other. The results showed that the minima could both be reliably detected as long as they had a phase separation of approximately $\Delta\phi \approx 0.33$. In the third test we applied the CPS to constant period data with different ratios of signal amplitude to noise in order to estimate the level of instability in the period estimation. We found increasing instability towards more noisy data and presented preliminary results for how this instability affects differential rotation estimation from light curve period variations.

The paper also includes a real world case study of 12 years of standard Johnson V band time series photometry from the young solar-type star NQ UMa (= HD 116956) using the CPS. The analysis revealed the star to have two remarkably stable active longitudes that had stayed intact for the full span of the observing record. A flip-flop event, where the main activity switched from one active longitude to the opposite, was identified between 1998 and 1999 and two smaller phase shifts at 2005–2006 and 2009. For the rest of the data, the active longitudes remained stable with the main spot activity located at one longitude and a secondary concentration on the opposite side of the star. The mean magnitude estimates suggested the possible presence of an activity cycle of approximately $P_{\rm cyc} \approx 3$ yr and the fluctuations seen in the photometric period estimates pointed at a moderate surface differential rotation coefficient of perhaps half of that seen on the Sun. We, furthermore, investigated the estimated mean time scale of change for the light curve fits and compared this to the theoretical estimate for the convective turnover time within the star.

The author developed of the CPS algorithm together with L. Jetsu, T. Hackman, and P. Kajatkari, and was responsible for choosing the BIC for the model order selection. The author performed the numerical tests and the analysis of NQ UMa with the aid of L. Jetsu and T. Hackman and had the main responsibility in writing the manuscript.

6.2 Paper II

In Paper II we presented a detailed case study of 24 years of Johnson V band time series photometry of the very active young solar-type star LQ Hya using the CPS method. The modelled light curve mean M and amplitude A levels showed prominent systematic variations that pointed towards the possibility of a roughly $P_{\rm cyc} \approx 13$ yr cycle. However, the length of this cycle was not significantly shorter than the full time span of the photometry and the correlation between the M and A estimates was poor, making the characterization of this cycle difficult. Another shorter time scale quasiperiodic pattern with a period of roughly $P_{\rm cyc} \approx 2$ yr could also be seen in the M results. No pronounced systematic variations could be seen in the photometric period estimates, which rather displayed apparently random fluctuations. These fluctuations pointed at weak surface differential rotation.

The rotation phase distribution of the light curve showed two kinds of behaviour depending on whether they were investigated globally or in shorter windows. Within the individual observing seasons there was commonly at least moderate phase coherence in the light curve minima. This phase coherence was for the most part lost in the global picture and the light curve minima appeared randomly across the whole rotation. Stable active longitudes could be seen only from 2003 to 2008 and possibly also for some years before 1995. For the rest of the time, the observed inter-seasonal phase stability appears

to have simply been connected to the life times of individual prominent active regions.

The author was responsible for performing the analysis and writing the manuscript.

6.3 Paper III

In Paper III the CPS was applied to 14 years of Johnson V band time series photometry of the young solar-type star V352 CMa. This star has a very low light curve amplitude and it provides a good example of how the CPS performs in cases where the periodic light curve signal is nearly drowned in the observational errors. We detected periodicity in 63% of the analyzed datasets and the performance of the CPS in deciding between the periodic and non-periodic model fits seemed to agree well with qualitative inspection of the data. We compared the period analysis results of the CPS to a periodogram analysis with the Horne-Baliunas method. The comparison revealed the two period search methods to agree well for the datasets where the CPS had determined a sinusoidal model fit, but the agreement between the detected periods was lost for datasets requiring a more complex model shape. This demonstrates the need to not restrict oneself to simple sinusoidal models when doing period analysis for active star photometry. The results of the CPS analysis suggested that the star has moderate differential rotation and an activity cycle of $P_{\mathrm{cyc}} = 11.7$ yr. We also detected an active longitude structure in the light curve minimum phases between 1998 and 2009.

This paper was based on the work done during the course "Variable stars" at the University of Helsinki in spring 2012 to which the author participated. The author was responsible in running the final CPS analysis and provided comments for the manuscript.

6.4 Paper IV

In Paper IV a detailed analysis of 32 years of Johnson V band time series photometry of LQ Hya was presented using the CF method. These results were compared to time series analysis done using the CPS, as well as to DI temperature maps produced by Cole et al. (2015) for 1998–2002.

Special care was taken in the paper to determine the mean photometric period of the star in the search for the optimal carrier wave frequency for the CF analysis. The period search results using both least-squares fitting and phase dispersion analysis revealed broad ranges of frequency values. The distribution of the detected frequencies was furthermore found to be multimodal, especially when using phase dispersion analysis with long correlation lengths for the included data point pairs. A symmetric and single peaked frequency distribution was only achieved when using phase dispersion analysis with correlation lengths shorter than approximately 230 d. This pattern was interpreted so that only on shorter time scales the periodogram is dominated by the mean pattern of spot motions, while on longer time scales the method tries to identify weaker longer lived structures and the symmetric frequency distribution break down. As a comparison, the resulting mean period from the phase dispersion analysis was very nearly the same as the weighted mean period obtained for the star in Paper II.

The CF analysis provided a model for how the light curve minimum phases have evolved on the star over the course of the observations. The results showed good agreement with the CPS results and decent agreement with the spot phases extracted from the DI maps. Similarly to Paper II, two periods with stable active longitudes could be identified, one from 1990 to 1994 and another from 2003 to 2009. Outside

of these time intervals there was little phase coherence and the local period associated with the light curve minima varied quickly. This variation could be explained with surface differential rotation and was consistent with previously published results. A total of seven fast flip-flop like phase jumps could be identified from the results. Four of these occurred during observing seasons and could be modelled with local CF analysis. However, only one of these, happening in 1992, occurred during the sections of the data with more stable active longitude patterns and even it happened between two observing seasons. There was no sign of periodicity between the identified flip-flop events.

The author provided the CPS results for the paper and commented on the manuscript, especially on the relation between the CF and the CPS results.

6.5 Paper V

Paper V concluded the photometric study of the young solar-type stars, including the CPS analysis of combined Johnson B and V band photometry from 21 stars gathered over 16 to 27 years. We also extended the estimation of the level of spurious period fluctuations in the model fits from the work done in Paper I. The improved estimate included the effects of observational noise, the number of data points, and the length of the datasets. We found that the quantified level of spurious period variations was in the order of a few percent of the actually observed variations for all of the sample stars, and thus the modelling uncertainties did not dominate our differential rotation estimates. Nevertheless, we concluded that the differential rotation estimates based on the level of the observed period fluctuation can have individually considerable uncertainties, and are better suited for population studies investigating the scaling of the differential rotation as a function of other stellar parameters. In line with previously published research, we found that the relative differential rotation coefficient k increases towards longer rotation periods. The relation of the absolute differential rotation shear $\Delta\Omega$ to the rotation rate Ω was less clear, but could be understood to indicate a nearly constant $\Delta\Omega$ for all rotation rates. We found no connection between $\Delta\Omega$ and the temperature of the stars, which was consistent with the theoretical results of Küker & Rüdiger (2011).

On 11 of the stars, we found active longitudes that remained stable for at least part of the length of the data. The active longitudes were frequently observed to have phase jumps and migration patterns and for some stars flip-flop events were identified. However, little or no regularity could be seen in any of these patterns, nor in the switches between active longitudes and random phase distribution of the activity, which were seen on some of the stars. For seven of the stars, we found evidence that the period $P_{\rm al}$ associated with the active longitudes has a different value than the mean photometric period $P_{\rm w}$. In these cases the active longitude periods were systematically shorter than the mean photometric periods. This discrepancy between the periods could be interpreted in a couple of ways. Either the active longitudes are anchored deeper in the stellar interiors, being subject to radial differential rotation, or they are manifestations of a non-axisymmetric dynamo mode exhibiting an azimuthal dynamo wave. The most striking feature in the active longitudes was their occurrence on stars according to their activity levels. With only two exceptions, all the stars where active longitudes were detected had chromospheric emission levels above $\log R'_{\rm HK} = -4.46$, while stars with no active longitudes had emission levels below this. The transition between the two regions appeared very sharp, indicating a probable connection to a domain shift between dynamo modes defined by axisymmetric and non-axisymmetric magnetic field configurations.

Activity cycles could be detected from the M and A results and their composites $M - A/2$ and $M + A/2$ for nearly all of the sample stars, a total of 18 out of the 21. On three stars we found quantifiable evidence for two simultaneous cycles of different periods $P_{\rm cyc}$. The stars could be placed onto the sequence of activity branches defined by Saar & Brandenburg (1999), when the ratio of rotation to cycle periods $P_{\rm rot}/P_{\rm cyc}$ was investigated as a function of either the inverse Rossby number Ro^{-1} or the chromospheric emission level $\log R'_{\rm HK}$. Our stars fell on the turnoff point between the "Active" and "Transitional" branches of Saar & Brandenburg (1999), demonstrating that these branches meet each other in a continuous manner. Our results also revealed two parallel subbranches within these previously detected main branches. The subbranches seem to indicate distinct cycle modes that a dynamo can excite, and the three stars having two detected cycles each had them on the different subbranches. The turnoff point between the "Active" and "Transitional" branches is close to the domain border between stars with and without active longitudes. This suggests a deeper connection in the level of dynamo action between the realized activity dependence of the cycle lengths and the excitation of axisymmetric or non-axisymmetric dynamo modes.

The author was responsible for reducing the spectroscopy, performing the analysis, and writing the manuscript. The spectroscopy was observed by the author at the NOT between 2012 and 2014.

7 Conclusions and future prospects

The work done for this thesis presents a detailed study of the spot activity on a sample of young solar-type stars, based on multidecadal and mostly continuous photometric monitoring. This data was investigated using a variety of time series analysis methods, which offer together a powerful tool set for investigating the rotation, active longitudes and activity cycles of the stars. The main focus of the work was in the analysis of the photometry, but the study was supplemented by measurements of the chromospheric Ca II H&K emission from high resolution spectroscopy. These measurements provided useful estimates of the activity levels of each of the sample stars.

The main results of this thesis concern differential rotation, the lengths of activity cycles, and the behaviour of the active longitudes. From the short scale dataset to dataset variations of the photometric rotation period, we uncovered evidence that the relative differential rotation coefficient k decreases towards the faster rotating stars. This result is in line with previously published studies. Likewise, comparing our results to the previous results, it seems quite safe to assume that the absolute rotational shear $\Delta\Omega$ due to surface differential rotation depends only weakly or not at all on the rotational velocity of the star. We did not find any evidence for the temperature dependence of differential rotation on the stars in our sample, which also agrees with other recent research for stars cooler than 6000 K. All in all, we did not get any new results concerning stellar differential rotation but did confirm older results with a new sample of stars.

Activity cycles could be detected from nearly all of the studied stars. When the ratio of rotation to cycle period, $P_{\mathrm{rot}}/P_{\mathrm{cyc}}$, was compared to the inverse Rossby number and the chromospheric emission index $\log R'_{\mathrm{HK}}$ of the stars, the estimated cycle periods revealed a clearly ordered behaviour. The activity cycles of stars with different rotation rates or activity levels appear to fall on distinct activity branches. In the case of stars where two different cycle periods where detected, these cycles always fell on two parallel branches. Our sample included stars from both sides of the turnoff point between two branches that show an opposite dependence of the cycle lengths from the Rossby number. Thus they help us thus to accurately locate this point of a potentially significant transition between two different dynamo regimes. Our results also revealed a previously unknown split into two parallel subbranches, that are visible at least on the more active side of the previously mentioned turnoff point. Satisfactory explanations of both the the forms of the activity branches and the transitions between them are not currently available and they require further work.

Active longitudes also turned out to be very common on sufficiently active stars. We found that practically all stars with a chromospheric activity level above $\log R'_{\mathrm{HK}} = -4.46$ have at least episodic active longitudes. On the less active side of this divide conclusive evidence for the non-axisymmetric distribution of spot activity was only found on one star, which itself is only barely less active than the other stars showing non-axisymmetry in the form of active longitudes. The location of the divide between the stars with axisymmetric and non-axisymmetric spot distributions is very near to the

turnoff point between the activity branches showing opposite cycle length dependence from the Rossby number. There is thus reason to suspect that both of these phenomena originate from the same shift in the types of dynamo modes acting in the stars. Dynamos operating in faster rotating, and thus more active, stars are known from simulations to prefer non-axisymmetric modes, but a connection to different cycle lengths has not yet been done. Also the episodic occurrence of active longitudes on some stars mixed with periods of axisymmetric spot distribution requires an explanation.

On seven of the stars we found evidence that the rotation period of the active longitudes does not coincide with the photometrically determined mean rotation period of the star. In all of these cases the active longitude period turned out to be shorter than the stellar rotation period. It may be that the magnetic structures generating the active longitudes are tracing the rotation of deeper layers in the stellar interiors, providing information of the radial differential rotation. On the other hand, the active longitudes may be the manifestations of azimuthal dynamo waves that are not anchored to the stellar plasma at all, but rotate with a differential phase velocity with respect to it. Such longitudinally propagating solutions are known from dynamo models but their relation to the actual observed values of active longitude periods as well as to the variable migration patterns seen on some stars still requires further work.

On some stars we found flip-flop events, where the location of the strongest activity switches relatively fast from one active longitude to another. There did not appear to be any regularity in how or when the flip-flops occurred. We certainly did not find any regular flip-flop cycles that have been discussed in many past studies. There still remain many open questions on the nature of the flip-flops, including the correct interpretation of each observationally detected event. What we might see as a flip-flop in the photometric record does not necessarily have to correspond to an activity switch between two physically present active longitudes. They can alternatively be caused, for example, by two spots rotating differentially with respect to each other, causing a beating pattern in the light curve. Any future study investigating flip-flops has to place special emphasis on this issue.

This study shows the importance of long records of continuous time series observations for the study of stellar activity. This is especially true for finding and characterizing activity cycles, which often have periods longer than a decade. They will simply not be detectable from any shorter time series. Even the study of active longitudes and flip-flops, which do not require as long stretches data to be reliably identified, benefits from extended monitoring. Patterns of changing behaviour, like variable migration rates of the active longitudes or the switching between axisymmetric and non-axisymmetric activity distribution, only become apparent after observing the same stars for extended periods of time. Our results show that new behaviour can be observed on stars even after monitoring them for decades.

It is hoped that programmes of both photometric and spectroscopic monitoring of spot and chromospheric activity will continue uninterrupted into the future to increase our knowledge of the long time scale activity patterns on stars. The solar analogy shows that there are activity patterns, like the Gleissberg cycle or the grand minima, which operate in the centennial time scales. It will hopefully some day be possible to perform detailed studies of these on other active stars as well. Meanwhile, there is room to develop progressively more sophisticated and robust analysis methods for the time series data. The commonly seen non-stationary nature of the activity signals still poses its problems for the currently used analysis tools.

It is also desirable that repeated detailed surface maps will be made through DI,

when possible, from the same stars that are included in the photometric or chromospheric monitoring programmes. These can provide detailed spatial information of the spot structures that is not detectable from photometry alone. At the same time the comparison to simultaneous photometry will increase the robustness of interpreting the DI results. The increasing availability of magnetic maps by ZDI is particularly welcome. Mapping the magnetic field structures can finally bridge the gap between the rather easily observed activity proxies and the dynamo models describing the evolution of the magnetic fields. Hopefully in the future more telescopes will get capabilities for the high resolution spectropolarimetry needed for ZDI.

Bibliography

Applegate, J. H. 1992, The Astrophysical Journal, 385, 621

Bai, T. 1988, The Astrophysical Journal, 328, 860

Baliunas, S. L., Donahue, R. A., Soon, W. H., et al. 1995, The Astrophysical Journal, 438, 269

Barnes, J. R., Collier Cameron, A., Donati, J.-F., et al. 2005, Monthly Notices of the Royal Astronomical Society, 357, L1

Barnes, T. G., Evans, D. S., & Moffett, T. J. 1978, Monthly Notices of the Royal Astronomical Society, 183, 285

Beck, J. G. 2000, Solar Physics, 191, 47

Berdyugina, S. V. 2005, Living Reviews in Solar Physics, 2, 8

Berdyugina, S. V., Pelt, J., & Tuominen, I. 2002, Astronomy & Astrophysics, 394, 505

Berdyugina, S. V., & Tuominen, I. 1998, Astronomy & Astrophysics, 336, L25

Böhm-Vitense, E. 2007, The Astrophysical Journal, 657, 486

Bopp, B. W., & Fekel, Jr., F. 1977, The Astronomical Journal, 82, 490

Bopp, B. W., & Stencel, R. E. 1981, The Astrophysical Journal Letters, 247, L131

Braithwaite, J. 2014, in Proceedings of the International Astronomical Union, Vol. 302, Magnetic Fields throughout Stellar Evolution, ed. P. Petit, M. Jardine, & H. C. Spruit, 255

Brandenburg, A., Saar, S. H., & Turpin, C. R. 1998, The Astrophysical Journal Letters, 498, L51

Brown, S. F., Donati, J.-F., Rees, D. E., & Semel, M. 1991, Astronomy & Astrophysics, 250, 463

Budding, E. 1977, Astrophysics and Space Science, 48, 207

Bumba, V., & Howard, R. 1965, The Astrophysical Journal, 141, 1502

Charbonneau, P. 2010, Living Reviews in Solar Physics, 7, 3

Cole, E., Käpylä, P. J., Mantere, M. J., & Brandenburg, A. 2014, The Astrophysical Journal Letters, 780, L22

Cole, E. M., Hackman, T., Käpylä, M. J., et al. 2015, Astronomy & Astrophysics, 581, A69

Collier Cameron, A. 2007, Astronomische Nachrichten, 328, 1030

Collier Cameron, A., Li, J., & Mestel, L. 1991, in NATO Advanced Science Institutes (ASI) Series C, Vol. 340, Angular Momentum Evolution of Young Stars, ed. S. Catalano & J. R. Stauffer (Springer), 297

Cox, A. N. 2000, Allen's astrophysical quantities (Springer: New York)

Croll, B., Walker, G., Kusching, R., et al. 2006, The Astrophysical Journal, 648, 607

Dobson, A. K., Donahue, R. A., Radick, R. R., & Kadlec, K. L. 1990, in Astronomical Society of the Pacific Conference Series, Vol. 9, Cool Stars, Stellar Systems, and the Sun, ed. G. Wallerstein, 132

Donahue, R. A., Saar, S. H., & Baliunas, S. L. 1996, The Astrophysical Journal, 466, 384

Donati, J.-F., Brown, S. F., Semel, M., et al. 1992, Astronomy & Astrophysics, 265, 682

Donati, J.-F., & Collier Cameron, A. 1997, Monthly Notices of the Royal Astronomical Society, 291, 1

Eberhard, G., & Schwarzschild, K. 1913, The Astrophysical Journal, 38, 292

Eddy, J. A. 1976, Science, 192, 1189

ESA, ed. 1997, ESA Special Publication, Vol. 1200, The HIPPARCOS and TYCHO catalogues. Astrometric and photometric star catalogues derived from the ESA HIPPARCOS Space Astrometry Mission

Eyer, L., & Bartholdi, P. 1999, Astronomy & Astrophysics Supplement Series, 135, 1

Fares, R. 2014, in Proceedings of the International Astronomical Union, Vol. 302, Magnetic Fields throughout Stellar Evolution, ed. P. Petit, M. Jardine, & H. C. Spruit, 180

Fares, R., Donati, J.-F., Moutou, C., et al. 2009, Monthly Notices of the Royal Astronomical Society, 398, 1383

Fröhlich, H.-E., Frasca, A., Catanzaro, G., et al. 2012, Astronomy & Astrophysics, 543, A146

Gaidos, E. J. 1998, Publications of the Astronomical Society of the Pacific, 110, 1259

Gaidos, E. J., Henry, G. W., & Henry, S. M. 2000, The Astronomical Journal, 120, 1006

Gleissberg, W. 1939, The Observatory, 62, 158

Gray, D. F. 1989, The Astrophysical Journal, 347, 1021

Gray, R. O., Corbally, C. J., Garrison, R. F., et al. 2006, The Astronomical Journal, 132, 161

Gray, R. O., Corbally, C. J., Garrison, R. F., McFadden, M. T., & Robinson, P. E. 2003, The Astronomical Journal, 126, 2048

Gray, R. O., Napier, M. G., & Winkler, L. I. 2001, The Astronomical Journal, 121, 2148

Haber, D. A., Hindman, B. W., Toomre, J., et al. 2000, Solar Physics, 192, 335

Hackman, T., Lehtinen, J., Rosén, L., Kochukhov, O., & Käpylä, M. J. 2016, Astronomy & Astrophysics, 587, A28

Hackman, T., Mantere, M. J., Lindborg, M., et al. 2012, Astronomy & Astrophysics, 538, A126

Hackman, T., Pelt, J., Mantere, M. J., et al. 2013, Astronomy & Astrophysics, 553, A40

Hale, G. E. 1908, The Astrophysical Journal, 28, 315

Hale, G. E., Ellerman, F., Nicholson, S. B., & Joy, A. H. 1919, The Astrophysical Journal, 49, 153

Hall, D. S. 1976, in IAU Colloq. 29: Multiple Periodic Variable Stars, ed. W. S. Fitch, Vol. 60, 287

Hall, D. S. 1991, in IAU Colloq. 130: The Sun and Cool Stars. Activity, Magnetism, Dynamos, ed. I. Tuominen, D. Moss, & G. Rüdiger, Vol. 380, 353

Hall, J. C. 2008, Living Reviews in Solar Physics, 5, 2

Hall, J. C., & Lockwood, G. W. 1995, The Astrophysical Journal, 438, 404

Haran, M. 2011, in Handbook of Markov Chain Monte Carlo, ed. S. Brooks, A. Gelman, G. L. Jones, & X.-L. Meng (Boca Raton: CRC Press), 449

Hathaway, D. H. 2015, Living Reviews in Solar Physics, 12, 4

Henry, G. W. 1995, in Astronomical Society of the Pacific Conference Series, Vol. 79, Robotic Telescopes. Current Capabilities, Present Developments, and Future Prospects for Automated Astronomy, ed. G. W. Henry & J. A. Eaton, 44

Henry, G. W. 1999, Publications of the Astronomical Society of the Pacific, 111, 845

Henry, G. W., Eaton, J. A., Hamer, J., & Hall, D. S. 1995, The Astrophysical Journal Supplement Series, 97, 513

Henry, T. J., Soderblom, D. R., Donahue, R. A., & Baliunas, S. L. 1996, The Astronomical Journal, 111, 439

Holzwarth, V., & Schüssler, M. 2003, Astronomy & Astrophysics, 405, 303

Horne, J. H., & Baliunas, S. L. 1986, The Astrophysical Journal, 302, 757

Howard, R. F. 1994, in Astronomical Society of the Pacific Conference Series, Vol. 68, Solar Active Region Evolution: Comparing Models with Observations, ed. K. S. Balasubramaniam & G. W. Simon, 1

Howe, R., Christensen-Dalsgaard, J., Hill, F., et al. 2000, Science, 287, 2456

Jetsu, L. 1993, Astronomy & Astrophysics, 276, 345

Jetsu, L. 1996, Astronomy & Astrophysics, 314, 153

Jetsu, L., Kokko, M., & Tuominen, I. 1992, Astronomy & Astrophysics, 265, 547

Jetsu, L., & Pelt, J. 1996, Astronomy & Astrophysics Supplement Series, 118, 587

Jetsu, L., & Pelt, J. 1999, Astronomy & Astrophysics Supplement Series, 139, 629

Jetsu, L., Pelt, J., & Tuominen, I. 1993, Astronomy & Astrophysics, 278, 449

Kajatkari, P., Jetsu, L., Cole, E., et al. 2015, Astronomy & Astrophysics, 577, A84

Karak, B. B., Käpylä, P. J., Käpylä, M. J., et al. 2015, Astronomy & Astrophysics, 576, A26

Kővári, Z., Strassmeier, K. G., Granzer, T., et al. 2004, Astronomy & Astrophysics, 417, 1047

Kővári, Z., Kriskovics, L., Künstler, A., et al. 2015, Astronomy & Astrophysics, 573, A98

Korhonen, H., Berdyugina, S. V., Hackman, T., et al. 1999, Astronomy & Astrophysics, 346, 101

Korhonen, H., Berdyugina, S. V., & Tuominen, I. 2002, Astronomy & Astrophysics, 390, 179

Krause, F., & Rädler, K.-H. 1980, Mean-field magnetohydrodynamics and dynamo theory (Oxford: Pergamon Press)

Kron, G. E. 1947, Publications of the Astronomical Society of the Pacific, 59, 261

Kuiper, N. 1960, in Proc. Koningkl. Nederl. Akad. Van Wettenschappen, Ser. A, Vol. 63, 38

Küker, M., & Rüdiger, G. 2011, Astronomische Nachrichten, 332, 933

Lehtinen, J., Jetsu, L., Hackman, T., Kajatkari, P., & Henry, G. W. 2011, Astronomy & Astrophysics, 527, A136

Lehtinen, J., Jetsu, L., Hackman, T., Kajatkari, P., & Henry, G. W. 2012, Astronomy & Astrophysics, 542, A38

Lehtinen, J., Jetsu, L., Hackman, T., Kajatkari, P., & Henry, G. W. 2016, Astronomy & Astrophysics, 588, A38

Lindborg, M., Korpi, M. J., Hackman, T., et al. 2011, Astronomy & Astrophysics, 526, A44

Lindborg, M., Mantere, M. J., Olspert, N., et al. 2013, Astronomy & Astrophysics, 559, A97

Lomb, N. 1976, Astrophysics and Space Science, 39, 447

Marsden, S. C., Petit, P., Jeffers, S. V., et al. 2014, Monthly Notices of the Royal Astronomical Society, 444, 3517

Messina, S., Guinan, E. F., Lanza, A. F., & Ambruster, C. 1999, Astronomy & Astrophysics, 347, 249

Middelkoop, F. 1982, Astronomy & Astrophysics, 107, 31

Montes, D., López-Santiago, J., Gálvez, M. C., et al. 2001, Monthly Notices of the Royal Astronomical Society, 328, 45

Morin, J., Donati, J.-F., Petit, P., et al. 2011, in IAU Symposium, Vol. 273, IAU Symposium, ed. D. Prasad Choudhary & K. G. Strassmeier, 181

Mézières, J.-C., & Christin, P. 1998, L'Orphelin des Astres (Paris: Dargaud)

Noyes, R. W., Hartmann, L. W., Baliunas, S. L., Duncan, D. K., & Vaughan, A. H. 1984, The Astrophysical Journal, 279, 763

Oláh, K., Kolláth, Z., & Strassmeier, K. G. 2000, Astronomy & Astrophysics, 356, 643

Oláh, K., Kolláth, Z., Granzer, T., et al. 2009, Astronomy & Astrophysics, 501, 703

Olspert, N., Käpylä, M. J., Pelt, J., et al. 2015, Astronomy & Astrophysics, 577, A120

Ossendrijver, M. 2003, The Astronomy and Astrophysics Review, 11, 287

Pelt, J., Brooke, J. M., Korpi, M. J., & Tuominen, I. 2006, Astronomy & Astrophysics, 460, 875

Pelt, J., Olspert, N., Mantere, M. J., & Tuominen, I. 2011, Astronomy & Astrophysics, 535, A23

Piskunov, N. E., Tuominen, I., & Vilhu, O. 1990, Astronomy & Astrophysics, 230, 363

Rädler, K.-H. 1986, Astronomische Nachrichten, 307, 89

Reinhold, T., & Gizon, L. 2015, Astronomy & Astrophysics, 583, A65

Reinhold, T., Reiners, A., & Basri, G. 2013, Astronomy & Astrophysics, 560, A4

Rodonò, M., Messina, S., Lanza, A. F., Cutispoto, G., & Teriaca, L. 2000, Astronomy & Astrophysics, 358, 624

Rutten, R. G. M. 1984, Astronomy & Astrophysics, 130, 353

Saar, S. H., & Brandenburg, A. 1999, The Astrophysical Journal, 524, 295

Scargle, J. D. 1982, The Astrophysical Journal, 263, 835

Schmitt, J. H. M. M., Schröder, K.-P., Rauw, G., et al. 2014, Astronomische Nachrichten, 335, 787

Schrijver, C. J., Cote, J., Zwaan, C., & Saar, S. H. 1989, The Astrophysical Journal, 337, 964

Schröter, E. H. 1985, Solar Physics, 100, 141

Schwabe, M. 1844, Astronomische Nachrichten, 21, 233

Selam, S. O., & Demircan, O. 1999, Turkish Journal of Physics, 23, 301

Semel, M. 1989, Astronomy & Astrophysics, 225, 456

Snodgrass, H. B., & Ulrich, R. K. 1990, The Astrophysical Journal, 351, 309

Soderblom, D. R. 1991, in NATO Advanced Science Institutes (ASI) Series C, Vol. 340, Angular Momentum Evolution of Young Stars, ed. S. Catalano & J. R. Stauffer (Springer), 151

Stoica, P., & Selén, Y. 2004, IEEE Signal Processing Magazine, 21, 36

Strassmeier, K. G., & Bopp, B. W. 1992, Astronomy & Astrophysics, 259, 183

Strassmeier, K. G., Hall, D. S., Barksdale, W. S., Jusick, A. T., & Henry, G. W. 1990, The Astrophysical Journal, 350, 367

Tanner, R. W. 1948, Journal of the Royal Astronomical Society of Canada, 42, 177

Telting, J. H., Avila, G., Buchhave, L., et al. 2014, Astronomische Nachrichten, 335, 41

Tuominen, I., Berdyugina, S. V., & Korpi, M. J. 2002, Astronomische Nachrichten, 323, 367

Tuominen, I., Berdyugina, S. V., Korpi, M. J., & Rönty, T. 1999, in Astronomical Society of the Pacific Conference Series, Vol. 178, Stellar Dynamos: Nonlinearity and Chaotic Flows, ed. M. Nunez & A. Ferriz-Mas, 195

Usoskin, I. G. 2013, Living Reviews in Solar Physics, 10, 1

Usoskin, I. G., Berdyugina, S. V., & Poutanen, J. 2005, Astronomy & Astrophysics, 441, 347

Vaughan, A. H., Preston, G. W., & Wilson, O. C. 1978, Publications of the Astronomical Society of the Pacific, 90, 267

Vidotto, A. A., Fares, R., Jardine, M., Moutou, C., & Donati, J.-F. 2015, Monthly Notices of the Royal Astronomical Society, 449, 4117

Vogt, S. S., Penrod, G. D., & Hatzes, A. P. 1987, The Astrophysical Journal, 321, 496

Waite, I. A., Marsden, S. C., Carter, B. D., et al. 2015, Monthly Notices of the Royal Astronomical Society, 449, 8

White, R. J., Gabor, J. M., & Hillenbrand, L. A. 2007, The Astronomical Journal, 133, 2524

Wilson, O. C. 1978, The Astrophysical Journal, 226, 379

Wright, J. T., Marcy, G. W., Butler, R. P., & Vogt, S. S. 2004, The Astrophysical Journal Supplement Series, 152, 261

Zhao, J., Bogart, R. S., Kosovichev, A. G., Duvall, Jr., T. L., & Hartlep, T. 2013, The Astrophysical Journal Letters, 774, L29